Charged-boson fluid in two and three dimensions

V. Apaja and J. Halinen

Department of Physical Sciences, Theoretical Physics, University of Oulu, Linnanmaa, FIN-90570 Oulu, Finland

V. Halonen

Department of Physical Sciences, Theoretical Physics, University of Oulu, Linnanmaa, FIN-90570 Oulu, Finland
and Institut für Theoretische Physik, Johannes Kepler Universität Linz, A-4040 Linz, Austria

E. Krotscheck

Department of Physics, Texas A&M University, College Station, Texas 77843
and Institut für Theoretische Physik, Johannes Kepler Universität Linz, A-4040 Linz, Austria

M. Saarela

Department of Physical Sciences, Theoretical Physics, University of Oulu, Linnanmaa, FIN-90570 Oulu, Finland
and Institut für Theoretische Physik, Johannes Kepler Universität Linz, A-4040 Linz, Austria

We examine various properties of the two- and three-dimensional plasma of charged bosons over an extensive range of densities, especially in the previously less studied low-density regime using a microscopic, variational approach. We calculate the ground-state structure and energetics and compare both our analytical and numerical results with earlier theoretical work. Throughout the entire density regime investigated, good agreement with the results of several Monte Carlo calculations is obtained. Triplet correlations are found to be important for the consistency of the equation of state at high densities. To study excitations we then allow for *time-dependent* interparticle correlations. Special attention is paid to the question of a microscopic justification for the "local-field factor," and the consistency demands imposed by sum rules on microscopic excitation theories. Results for the static dielectric function $\epsilon(k,0)$ and the dynamic structure function $S(k,\omega)$ are presented in three and two dimensions. [S0163-1829(97)06119-5]

I. INTRODUCTION

The fluid of charged bosons embedded in a neutralizing background at $T=0$ has mostly been considered as a model many-body system in quantum statistical mechanics, which parallels the physically more significant fluid of electrons, but has no real physical applications. This picture has changed to some extent in recent years, especially after the discovery of high-temperature superconductivity in layered compounds and in certain ceramic materials. Interestingly, the three-dimensional charged-boson fluid has received attention as a model for superconductors even prior to the BCS theory,[1] but has since been mostly ignored until this recent revived interest.[2–6] In a sense, these two models are complementary.[7] The BCS theory is the appropriate approach if the coherence length is much larger than the mean distance between the particles, whereas the boson-fluid approach is suitable when the coherence length is of the order of the mean particle distance.

The main reason for disregarding the charged-boson fluid has been the fact that, unlike its fermionic counterpart, the electron gas, it has not been realized in a laboratory, although injecting deuterium up to a high density into metals such as palladium or vanadium may be a promising way to generate it. The charged-boson fluid has also astrophysical relevance[8–10] in the description of pressure-ionized helium in cold degenerate stellar matter. Recent interest has been in the fusion of three α particles in a dense helium plasma.[11,12]

Besides the possible applications, the fluid of charged bosons in two and three dimensions offers a relatively simple many-body model system. Microscopic many-body methods for this system have matured to a point where precise and unambiguous predictions can be made for the ground-state properties. This permits one to study the effects of dimensionality; it also imposes, as we shall argue, a revised view of excitation theories.

Early theoretical approaches to study this many-body problem have been based on the transformation technique developed by Bogoliubov or, equivalently, on the random phase approximation (RPA) scheme. These methods give a fairly good description in the high-density perturbative regime due to weak correlations (and high condensate fraction), but they fail severely when the correlation strength grows with decreasing density and the system resembles the ideal Bose gas less and less. Other approaches, which incorporate also the effects of strong interparticle correlations, include the scheme by Singwi *et al.*[13] (STLS) and several variational studies.[14,15]

There exists a number of calculations of the ground state and excitations of the three-dimensional system;[16–24] the two-dimensional (2D) system has been studied considerably less.[25–28] The dielectric properties[29–34] and static density response[35] of both of these systems have also attracted interest. A number of Monte Carlo simulations have been devoted to this subject, the most relevant from the viewpoint of the present study being the calculations by Hansen and

Mazighi[36] using a variational Monte Carlo approach, as well as those by Ceperley and Alder[37] and a very recent work by Moroni, Conti, and Tosi[38] with a diffusion Monte Carlo approach. In the first two studies the authors obtain the ground-state energy over an extensive range of densities including the Wigner crystal phase, while Moroni *et al.* also calculate the momentum distribution, dielectric response, and give bounds for excited states of the 3D plasma. Because the ground-state properties of these systems are quite well known, we feel that one should reexamine the excited states in view of this precise knowledge. Especially the diffusion Monte Carlo results provide useful information and pose an interesting challenge for the microscopic many-body theories.

The properties of the charged-boson fluid are characterized by a single dimensionless coupling parameter $r_s = r_0/a_0$, where a_0 is the Bohr radius and r_0 is the radius of a sphere (circle in two dimensions) that encloses on average one particle and is thus related to the number density ρ by

$$r_0 = \begin{cases} (\pi\rho)^{-1/2} & \text{(in 2D)} \\ (4\pi\rho/3)^{-1/3} & \text{(in 3D)}. \end{cases} \quad (1.1)$$

Depending on the density, three distinct physical regimes in these charged systems are characterized: starting from the weakly coupled fluid ($r_s \ll 1$) the interparticle correlations grow in strength and the system becomes gradually strongly coupled until it eventually undergoes a zero-temperature phase transition to form a Wigner crystal at low densities.

The purpose of this work is to study the charged-boson fluid in two and three dimensions using the well-tested and widely applied hypernetted-chain Euler-Lagrange (HNC/EL) formalism to calculate the structure and energetics of the ground state as well as the excited states of these systems. The next section reviews the basic formalism, including a comprehensive study of the triplet correlations and a comparison with parquet-diagram theory. Section III studies excitations and the dynamic structure function within a simple version of the correlated basis function (CBF) theory, which is derived using the method of time-dependent pair correlations. Special emphasis is placed on the analytic structure of the dynamic response function; this allows us to address the question of various ways to define a ''local-field factor'' and to study the compressibility consistency in the high-density limit.

II. GROUND-STATE STRUCTURE

A. Ground-state theory

The microscopic description of a strongly interacting quantum many-body system begins conventionally with the Hamiltonian

$$H = -\frac{\hbar^2}{2m}\sum_{i=1}^{N}\nabla_i^2 + \sum_{i<j} v(|\mathbf{r}_i - \mathbf{r}_j|). \quad (2.1)$$

In our case of the charged-boson fluid $v(|\mathbf{r}_i - \mathbf{r}_j|)$ is the Coulomb potential and the neutralizing background charge must be added into the Hamiltonian. In three dimensions the Coulomb interaction has the familiar form $v(r) \propto 1/r$. In two dimensions there are two well-defined Coulomb systems,

namely, the ''restricted three-dimensional'' or the quasi-two-dimensional fluid and the ''pure'' Coulomb fluid. The former consists of charges that interact via the $1/r$ potential, but which are confined to move in a plane. In the latter case the interaction is logarithmic. That is of particular interest as a many-body problem involving very long-range interactions since it is a quantum Bose fluid without a Bose condensate at zero temperature.[39,40] In this paper, however, we are interested in the quasi-two-dimensional fluid, which is a more realistic model for films of charged particles.

The ground-state wave function for a system of N identical bosons with coordinates $\mathbf{r}_1, \ldots, \mathbf{r}_N$ is written as a variational ansatz of the Jastrow-Feenberg form

$$\Psi_0(\mathbf{r}_1, \ldots, \mathbf{r}_N) = \exp\left[\frac{1}{2}\left\{\sum_{i<j} u_2(\mathbf{r}_i, \mathbf{r}_j)\right.\right.$$
$$\left.\left. + \sum_{i<j<k} u_3(\mathbf{r}_i, \mathbf{r}_j, \mathbf{r}_k) + \cdots\right\}\right]. \quad (2.2)$$

The most important component of the variational wave function is the two-body function $u_2(\mathbf{r}_i, \mathbf{r}_j)$, which describes both the short- and long-range correlations between pairs of particles. In fact, one of the reasons for the success of the variational theory is that it is *exact* in both the weakly interacting limit (in which case the theory reduces to the random phase approximation) *and* in the strongly interacting limit (in which case it reduces to the Bethe-Goldstone equation).

For all practical applications known so far, the restriction of the Feenberg function (2.2) to pair and triplet correlations has turned out to be sufficient. Moreover, the triplet correlations $u_3(\mathbf{r}_i, \mathbf{r}_j, \mathbf{r}_k)$ only improve the quantitative agreement between the theory and measurements or exact simulations but they do not change the essential features of the theory. The effect of triplet correlations has been studied thoroughly in helium systems,[41,42] where they are known to be important since the interparticle correlations are strong. The role of the triplet correlations in charged fluids has been less explored. In fact, there seems to be a general agreement that they can be safely neglected at the metallic densities. While this is numerically true, we shall see that triplet correlations are needed even in the high-density limit for consistency reasons.

An important aspect of the variational theory is the optimization of the correlations. The correlation functions are determined by the minimization of the energy-expectation value, formally written as

$$\frac{\delta}{\delta u_n}\left[\frac{\langle\Psi_0|H|\Psi_0\rangle}{\langle\Psi_0|\Psi_0\rangle}\right] = 0, \quad n = 2, 3. \quad (2.3)$$

The additional information needed to solve these equations is the connection between the correlation functions and the physically observable distribution functions. This connection is provided by the hypernetted-chain equations.[43] These equations are derived by diagrammatic analysis of the two-body distribution function $g(r)$ in terms of the two-body correlation function. The analysis leads to the HNC relationships

$$g(r) = \exp\{u_2(r) + N(r) + E(r)\}. \quad (2.4)$$

The function $E(r)$ represents an infinite series of "elementary" diagrams that can be expressed as multidimensional integrals involving $g(r)$. The sum of nodal diagrams, $N(r)$, can be expressed conveniently in momentum space. Introducing the dimensionless Fourier transform

$$\widetilde{f}(k) = \rho \int d^d r f(r) e^{i\mathbf{k}\cdot\mathbf{r}}, \tag{2.5}$$

where d denotes the dimensionality of the system, and the static structure function

$$S(k) = 1 + \rho \int d^d r e^{i\mathbf{k}\cdot\mathbf{r}}[g(r) - 1], \tag{2.6}$$

the function $\widetilde{N}(k)$ has the form

$$\widetilde{N}(k) = \frac{[S(k) - 1]^2}{S(k)} = \frac{\widetilde{X}^2(k)}{1 - \widetilde{X}(k)}, \tag{2.7}$$

where we have also introduced, for further reference, the "direct correlation function" or the "nonnodal function"

$$\widetilde{X}(k) = S(k) - 1 - \widetilde{N}(k). \tag{2.8}$$

The level of the HNC approximation is defined by the choice of $E(r)$; e.g., HNC/0 neglects the elementary diagrams altogether, note that triplet correlations can be implemented through a modification of the definition of "elementary diagrams." The combination of the HNC equations (2.4) and the Euler equations (2.3) are generally referred to as the hypernetted-chain Euler-Lagrange theory. With the quantities introduced above, the correlation energy can be written as

$$E = E_r + E_k + E_e + E_3 \tag{2.9}$$

with

$$\frac{E_r}{N} = \frac{\rho}{2} \int d^d r \left[[g(r) - 1] v(r) + \frac{\hbar^2}{m} \left| \nabla \sqrt{g(r)} \right|^2 \right], \tag{2.10}$$

$$\frac{E_k}{N} = -\frac{\hbar^2}{8m} \int \frac{d^d k}{(2\pi)^d \rho} k^2 [S(k) - 1] \widetilde{N}(k), \tag{2.11}$$

$$\frac{E_e}{N} = -\frac{\hbar^2}{8m} \int \frac{d^d k}{(2\pi)^d \rho} k^2 [S(k) - 1] \widetilde{E}(k), \tag{2.12}$$

and E_3 is the contribution from triplet correlations. This term can be expressed in terms of the three-body correlation function $u_3(\mathbf{r}_1, \mathbf{r}_2, \mathbf{r}_3)$ and the three-body distribution function. Our working formulas[44,45,41] displayed in the next subsection have turned out to be quite sufficient for all practical purposes.

The details of the HNC/EL scheme have been discussed in many contexts; for a comprehensive review of the method see Ref. 42. Previous applications have mostly focused on helium liquids, but the formalism is identical in the present case and does not need to be discussed in detail in this context. The Euler-Lagrange equation can be conveniently written in coordinate space for the radial distribution function,

$$-\frac{\hbar^2}{m} \nabla^2 \sqrt{g(r)} + [v(r) + \Delta V_{\text{ele}}(r) + w_{\text{ind}}(r)] \sqrt{g(r)}$$

$$= 0, \tag{2.13}$$

where the "induced interaction" is

$$\widetilde{w}_{\text{ind}}(k) = -\frac{\hbar^2 k^2}{2m}[S(k) - 1] - \frac{\hbar^2 k^2}{4m}\left[\frac{1}{S^2(k)} - 1\right]$$

$$= -\frac{\hbar^2 k^2}{2m}[S(k) - 1] - \widetilde{V}_{p\text{-}h}(k), \tag{2.14}$$

and $\Delta V_{\text{ele}}(r)$ is a term that arises from triplet correlations and elementary diagrams,

$$\Delta V_{\text{ele}}(r) = \frac{2}{N\rho} \frac{\delta(E_3 + E_e)}{\delta g(r)}. \tag{2.15}$$

The coordinate-space formulation of the Euler equation (2.13) is readily identified with the boson Bethe-Goldstone equation, which sums the dominant diagrams in the strong-coupling limit.

A formulation of the Euler-Lagrange equations to (2.13) can be given in momentum space in terms of the structure factor $S(k)$,

$$S(k) = \left\{ 1 + \frac{4m}{\hbar^2 k^2} \widetilde{V}_{p\text{-}h}(k) \right\}^{-1/2}. \tag{2.16}$$

This equation is formally identical to the boson-RPA expression for the structure factor; the HNC/EL theory supplements the RPA with a microscopic theory of the particle-hole interaction

$$V_{p\text{-}h}(r) = g(r)[v(r) + \Delta V_{\text{ele}}(r)] + \frac{\hbar^2}{m}|\nabla \sqrt{g(r)}|^2$$

$$+ [g(r) - 1]w_{\text{ind}}(r). \tag{2.17}$$

Thus the HNC/EL theory sums *both* important sets of diagrams self-consistently.

Equations (2.16), (2.17), and (2.14) can be solved iteratively for $g(r)$ and $S(k)$. We can then go back and calculate the ground-state energy from the expression (2.9) for the energy-expectation value.

The pressure of the system is calculated by varying the energy per particle with respect to the density. It can be expressed entirely in terms of the ground-state structure functions,
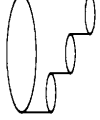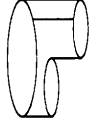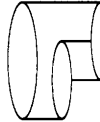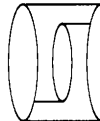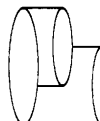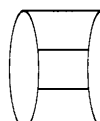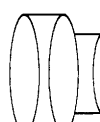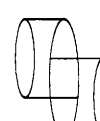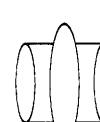
$$\frac{P}{\rho} = \rho \frac{dE/N}{d\rho}. \tag{2.18}$$

The chemical potential of the system is defined as $\mu = E/N + P/\rho$, and the hydrodynamic compressibility K_T is obtained by differentiating the chemical potential with respect to density

$$\frac{1}{\rho K_T} = \rho \frac{d\mu}{d\rho}. \tag{2.19}$$

Since the definition of the compressibility contains the second derivative of the energy one also needs to calculate the

TABLE I. All fourth-order perturbation theory diagrams are shown in their diagrammatic form (right column) and their analytic expression (left column). The middle column contains the analytic form of the HNC/EL approximation of the same diagrams. These results have been derived in Ref. 46.

Perturbation Theory	HNC/EL	
$-\dfrac{5}{16}\displaystyle\int \dfrac{d^3k}{(2\pi)^3\rho}\dfrac{\tilde{V}^4(k)}{t^3(k)}$	$-\dfrac{5}{16}\displaystyle\int \dfrac{d^3k}{(2\pi)^3\rho}\dfrac{\tilde{V}^4(k)}{t^3(k)}$	
$-\dfrac{1}{4}\displaystyle\int \dfrac{d^3k d^3p}{(2\pi)^6\rho^2}\dfrac{\tilde{V}^2(k)\tilde{V}(p)\tilde{V}(|\mathbf{p}+\mathbf{k}|)}{t^2(k)t(p)}$	$-\dfrac{1}{4}\displaystyle\int \dfrac{d^3k d^3p}{(2\pi)^6\rho^2}\dfrac{\tilde{V}^2(k)\tilde{V}(p)\tilde{V}(|\mathbf{p}+\mathbf{k}|)}{t^2(k)t(p)}$	
$-\dfrac{1}{4}\displaystyle\int \dfrac{d^3k d^3p}{(2\pi)^6\rho^2}\dfrac{\tilde{V}^2(k)\tilde{V}(p)\tilde{V}(|\mathbf{p}+\mathbf{k}|)}{t^2(k)(t(k)+t(p)+t(|\mathbf{p}+\mathbf{k}|))}$	$-\dfrac{1}{8}\displaystyle\int \dfrac{d^3k d^3p}{(2\pi)^6\rho^2}\dfrac{\tilde{V}^2(k)\tilde{V}(p)\tilde{V}(|\mathbf{p}+\mathbf{k}|)}{t^2(k)t(p)}$	
$-\dfrac{1}{4}\displaystyle\int \dfrac{d^3k d^3p}{(2\pi)^6\rho^2}\dfrac{\tilde{V}^2(k)\tilde{V}(p)\tilde{V}(|\mathbf{p}+\mathbf{k}|)}{t(k)t(p)(t(k)+t(p)+t(|\mathbf{p}+\mathbf{k}|))}$	$-\dfrac{3}{4}\displaystyle\int \dfrac{d^3k d^3p}{(2\pi)^6\rho^2}\dfrac{\tilde{V}^2(k)\tilde{V}(p)\tilde{V}(|\mathbf{p}+\mathbf{k}|)}{t(k)t(p)t(|\mathbf{p}+\mathbf{k}|)}$	
$-\dfrac{1}{2}\displaystyle\int \dfrac{d^3k d^3p}{(2\pi)^6\rho^2}\dfrac{\tilde{V}^2(k)\tilde{V}(p)\tilde{V}(|\mathbf{p}+\mathbf{k}|)}{t(k)t(p)(t(k)+t(p)+t(|\mathbf{p}+\mathbf{k}|))}$	– – –	
$-\dfrac{1}{16}\displaystyle\int \dfrac{d^3k d^3p d^3q}{(2\pi)^9\rho^3}\dfrac{\tilde{V}(k)\tilde{V}(p)\tilde{V}(q)}{t(k)t(p)t(q)}$	$-\dfrac{1}{16}\displaystyle\int \dfrac{d^3k d^3p d^3q}{(2\pi)^9\rho^3}\dfrac{\tilde{V}(k)\tilde{V}(p)\tilde{V}(q)}{t(k)t(p)t(q)}$	
$-\dfrac{1}{4}\displaystyle\int \dfrac{d^3k d^3p}{(2\pi)^6\rho^2}\dfrac{\tilde{V}^2(k)\tilde{V}^2(p)}{t^2(k)(t(k)+t(p)+t(|\mathbf{p}+\mathbf{k}|))}$	– – –	
$-\dfrac{1}{4}\displaystyle\int \dfrac{d^3k d^3p}{(2\pi)^6\rho^2}\dfrac{\tilde{V}^2(k)\tilde{V}^2(p)}{t(k)t(p)(t(k)+t(p)+t(|\mathbf{p}+\mathbf{k}|))}$	– – –	
$\dfrac{1}{8}\displaystyle\int \dfrac{d^3k d^3p}{(2\pi)^6\rho^2}\dfrac{\tilde{V}^2(k)\tilde{V}^2(p)}{t^2(k)t(p)}$	– – –	

linear response of the ground-state structure functions to density variations. We will return to this problem when the static response function is evaluated.

B. Triplet correlations and parquet diagrams

The self-consistent summation of ring and ladder diagrams mentioned above has been used and exploited in the parquet-diagram theory.[46–50] One of the important conclu-

sions of that theory is that HNC/EL sums not only all ring and ladder diagrams exactly, but also mixed diagrams in a local approximation and provides a precise prescription on how the HNC/EL theory is obtained from perturbation theory. Furthermore, Jackson *et al.* have shown[46] that discrepancies between the exact perturbation expansion and the diagrams summed by the HNC/EL equation appear in fourth order in the potential. The purpose of this section is to study

how the statement of Ref. 46 is generalized if triplet correlations are included in the HNC/EL scheme.

Table I (from Ref. 46) shows all fourth-order perturbation-theory diagrams together with all terms of fourth order in the potential generated by iterating the HNC/EL equations. We can now calculate the *difference* between the full perturbation-theory expression (i.e., the sum of all terms in the first column of Table I) *and* the HNC/EL approximation (i.e., the sum of all terms in the second column of Table I). The calculation is somewhat tedious, but straightforward and leads to the compact result

$$-\frac{1}{24}\int \frac{d^dk\,d^dp\,d^dq}{(2\pi)^{2d}\rho^2}\,\delta(\mathbf{p}+\mathbf{k}+\mathbf{q})$$

$$\times\frac{|(\hbar^2/2m)[\mathbf{p}\cdot\mathbf{k}[\widetilde{V}(p)/t(p)][\widetilde{V}(k)/t(k)]+\mathbf{p}\cdot\mathbf{q}[\widetilde{V}(p)/t(p)]\widetilde{V}(q)/t(q)+\mathbf{k}\cdot\mathbf{q}[\widetilde{V}(k)/t(k)]\widetilde{V}(q)/t(q)]|^2}{t(p)+t(k)+t(q)}, \tag{2.20}$$

where $t(k)=\hbar^2k^2/2m$ and $\widetilde{V}(k)$ the bare interaction. This equation is to be compared with the three-body energy correction as derived, for example, in Refs. 44 or 41:

$$\frac{E_3}{N}=\frac{1}{24}\int\frac{d^dk\,d^dp\,d^dq}{(2\pi)^{2d}\rho^2}\delta(\mathbf{p}+\mathbf{k}+\mathbf{q})S(p)S(k)S(q)\widetilde{u}_3(\mathbf{k},\mathbf{p},\mathbf{q})\Bigg\{\frac{\hbar^2}{m}[\mathbf{p}\cdot\mathbf{k}\widetilde{X}(p)\widetilde{X}(k)+\mathbf{p}\cdot\mathbf{q}\widetilde{X}(p)\widetilde{X}(q)+\mathbf{k}\cdot\mathbf{q}\widetilde{X}(k)\widetilde{X}(q)]$$

$$+[\varepsilon(p)+\varepsilon(k)+\varepsilon(q)]\widetilde{u}_3(\mathbf{k},\mathbf{p},\mathbf{q})\Bigg\}. \tag{2.21}$$

Here $\varepsilon(k)$ is the Feynman excitation energy

$$\varepsilon(k)=\frac{\hbar^2k^2}{2mS(k)}, \tag{2.22}$$

and $\widetilde{u}_3(\mathbf{k},\mathbf{p},\mathbf{q})$ is the triplet correlation function or, more generally, the irreducible three-body vertex. The three-body energy is a quadratic functional of $\widetilde{u}_3$ and thus can be easily minimized, yielding

$$\widetilde{u}_3(\mathbf{k},\mathbf{p},\mathbf{q})=-\frac{(\hbar^2/2m)[\mathbf{k}\cdot\mathbf{p}\widetilde{X}(p)\widetilde{X}(k)+\mathbf{p}\cdot\mathbf{q}\widetilde{X}(p)\widetilde{X}(q)+\mathbf{k}\cdot\mathbf{q}\widetilde{X}(k)\widetilde{X}(q)]}{\varepsilon(k)+\varepsilon(p)+\varepsilon(q)}\delta(\mathbf{p}+\mathbf{k}+\mathbf{q}). \tag{2.23}$$

Inserting this result back to the three-body energy we get an expression that is very similar to Eq. (2.20),

$$\frac{E_3}{N}=-\frac{1}{24}\int\frac{d^dk\,d^dp\,d^dq}{(2\pi)^{2d}\rho^2}\delta(\mathbf{p}+\mathbf{k}+\mathbf{q})S(p)S(k)S(q)\frac{|(\hbar^2/2m)[\mathbf{p}\cdot\mathbf{k}\widetilde{X}(p)\widetilde{X}(k)+\mathbf{p}\cdot\mathbf{q}\widetilde{X}(p)\widetilde{X}(q)+\mathbf{k}\cdot\mathbf{q}\widetilde{X}(k)\widetilde{X}(q)]|^2}{\varepsilon(k)+\varepsilon(p)+\varepsilon(q)}. \tag{2.24}$$

The identity of the triplet energy (2.24) with the fourth-order correction (2.20) is now easily verified, to leading order in the interaction, by expanding the direct correlation function (2.8),

$$\widetilde{X}(k)=1-S^{-1}(k)\approx-\frac{\widetilde{V}(k)}{t(k)} \tag{2.25}$$

and replacing the Feynman spectrum $\varepsilon(k)$ by the kinetic energy $t(k)$. Thus, we have shown that HNC/EL and parquet theory are identical and exact to at least fourth order in the potential when triplet correlations or three-body vertex functions are included. We conjecture here that the identity extends to fifth order in the potential since the first elementary diagram is of sixth order. The distinction between HNC/EL and parquet theory is, thus, also at the next order a matter of language and derivation, but not of physical content. As a matter of practicality we note that the triplet energy in the variational approach results directly in a closed-form expression,[44] whereas it appears by no means obvious that the diagrams shown in Table I can be combined in such a compact manner. We also note that Jackson *et al.* report large-scale cancellations between the individual diagrams.[50]

The three-body vertex also gives a contribution to the particle-hole potential, which will be needed below. It is conveniently calculated in the momentum space,

$$\Delta\widetilde{V}_{p\text{-}h}^{(3)}(k)=2\frac{\delta E_3}{\delta S(k)}=\frac{1}{4}\int\frac{d^dp\,d^dq}{(2\pi)^d\rho}\delta(\mathbf{p}+\mathbf{k}+\mathbf{q})S(p)S(q)\widetilde{u}_3(\mathbf{k},\mathbf{p},\mathbf{q})\Bigg\{\frac{\hbar^2}{m}[\mathbf{k}\cdot\mathbf{p}\widetilde{X}(p)+\mathbf{k}\cdot\mathbf{q}\widetilde{X}(q)+\mathbf{p}\cdot\mathbf{q}\widetilde{X}(p)\widetilde{X}(q)]$$

$$+[\varepsilon(p)+\varepsilon(q)]\widetilde{u}_3(\mathbf{k},\mathbf{p},\mathbf{q})\Bigg\}. \tag{2.26}$$

C. Uniform limit approximation

The two formulations of the Euler equation (2.13) and (2.16) serve an important purpose: as already pointed out, Eq. (2.16) is a boson-RPA equation, in other words, the HNC/EL theory sums all ring diagrams that dominate the energy in the high-density limit. For further reference, and to see that one actually obtains the RPA energy in that limit, we make the so-called "uniform limit approximation."[43] The approximation assumes that all pair functions are small in coordinate space, but can be long ranged and therefore large in momentum space. The approximation amounts, in Eq. (2.9), to expanding the term $\sqrt{g(r)}$ in the form

$$\sqrt{g(r)} \approx 1 + \tfrac{1}{2}[g(r) - 1]. \qquad (2.27)$$

This leads, after a few manipulations (note that we ignore, in this limit, elementary diagrams and triplet correlations), to the expression

$$\frac{E_{RPA}}{N} = \frac{1}{2} \int \frac{d^d k}{(2\pi)^d \rho} [S(k) - 1] \left[\tilde{v}(k) + \frac{\hbar^2 k^2}{4m} [1 - S^{-1}(k)] \right]$$

$$\equiv \frac{V_{RPA}}{N} + \frac{T_{RPA}}{N}. \qquad (2.28)$$

Here we have also defined, for further reference, the uniform limit approximation of the kinetic energy,

$$\frac{T_{RPA}}{N} = \frac{\hbar^2}{8m} \int \frac{d^d k}{(2\pi)^d \rho} k^2 \frac{[S(k) - 1]^2}{S(k)}. \qquad (2.29)$$

If we furthermore use the Coulomb interaction instead of the full particle-hole interaction in Eq. (2.16) we readily see that the expression for E_{RPA}/N is identical to the energy obtained by coupling-constant integration in the RPA,

$$\frac{E_{RPA}}{N} = \frac{1}{2} \int \frac{d^d k}{(2\pi)^d \rho} \tilde{v}(k) \int_0^1 d\lambda [S_\lambda(k) - 1], \quad (2.30)$$

where $S_\lambda(k)$ is the structure function (2.16) with $\tilde{V}_{p\text{-}h}(k)$ replaced by the Coulomb potential $\lambda \tilde{v}(k)$.

D. Energetics and ground-state structure

We begin the discussion of the ground-state energetics and structure function with the high-density limit $r_s \to 0$. In that limit it is customary[16,51] to choose a new dimensionless variable for the wave number:

$$\xi = \begin{cases} k r_0 r_s^{-1/4} & (\text{in 3D}) \\ k r_0 r_s^{-1/3} & (\text{in 2D}). \end{cases} \qquad (2.31)$$

In the high-density limit the particle-hole interaction (2.17) is dominated by the bare Coulomb potential and the expressions for the structure functions become particularly simple:

$$S(\xi) = \frac{1}{\sqrt{1 + 12/\xi^4}} \quad (\text{in 3D}) \qquad (2.32)$$

$$S(\xi) = \frac{1}{\sqrt{1 + 8/\xi^3}} \quad (\text{in 2D}). \qquad (2.33)$$

The Fourier transform of the structure function, or more precisely of $S(\xi) - 1$, approaches zero like $r_s^{3/4}$ in the 3D case and like $r_s^{2/3}$ in the 2D case. Thus the radial distribution function approaches unity and the uniform limit approximation becomes valid. The total energy per particle as well as the chemical potential can then be expressed in terms of the structure function alone and the coefficients of the leading-order terms in the r_s expansion can be calculated,

$$E/N = \frac{2}{\pi} r_s^{-3/4} \int_0^\infty d\xi \frac{S(\xi) - 1}{S(\xi) + 1} = -0.803079 r_s^{-3/4} \text{ Ry},$$

$$\mu = \frac{2}{\pi} r_s^{-3/4} \int_0^\infty d\xi (S(\xi) - 1) = -1.00385 r_s^{-3/4} \text{ Ry}$$

$$(\text{in 3D}), \quad (2.34)$$

$$E/N = r_s^{-2/3} \int_0^\infty d\xi \frac{S(\xi) - 1}{S(\xi) + 1} = -1.29355 r_s^{-2/3} \text{ Ry},$$

$$\mu = r_s^{-2/3} \int_0^\infty d\xi (S(\xi) - 1) = -1.72474 r_s^{-2/3} \text{ Ry}$$

$$(\text{in 2D}). \quad (2.35)$$

These results are well known for the three-dimensional charged-boson gas.[16,51] The pressure and the compressibility calculated from the definitions (2.18) and (2.19) are then

$$P/\rho = \tfrac{1}{4} E/N, \quad 1/(\rho K_T) = \tfrac{1}{4} \mu \quad (\text{in 3D}), \qquad (2.36)$$

$$P/\rho = \tfrac{1}{3} E/N, \quad 1/(\rho K_T) = \tfrac{1}{3} \mu \quad (\text{in 2D}). \qquad (2.37)$$

These limits serve useful purposes for the design of interpolation formulas for the equation of state, and as a consistency test of numerical calculations at lower densities; we will return to them when we discuss the compressibility consistency.

Let us now turn to a discussion of our HNC/EL results over a wide density regime. The ground-state energies of the 3D system at several densities are given in Table II along with the results of several Monte Carlo calculations[38,37,36] and the STLS approach.[34] The agreement between our HNC/EL energies and those of Moroni *et al.* is typically better than 0.2%, which we consider quite satisfactory and sufficient for all practical purposes. There appear to be larger differences even in the results of the two diffusion Monte Carlo (DMC) calculations. The authors[38] assign this discrepancy to differences in the size extrapolation and convergence of the Ewald sums used in the calculations. The STLS approach gives also energies that are in fair agreement with the DMC results.

Table III shows the decomposition of the correlation energy into the HNC/0 contribution, and the correction terms originating from triplet correlations and elementary dia-

TABLE II. Ground-state energy E_g of the three-dimensional charged-boson fluid from the present calculation (including triplet correlations and elementary diagrams) compared with the diffusion Monte Carlo results by Moroni, Conti, and Tosi (MCT) (Ref. 38) and by Ceperley and Alder (CA) (Ref. 37). Also shown are the variational Monte Carlo results by Hansen and Mazighi (HM) (Ref. 36) and the results obtained through the STLS approach (Ref. 34).

r_s	E_g (full)	MCT	CA	HM	STLS
0.1	-4.48857				
1.0	-0.77675	$-0.77664(5)$		-0.7810	-0.771240
2.0	-0.45203	$-0.45192(3)$	-0.4531	-0.4547	-0.447180
5.0	-0.21657	$-0.216420(12)$	$-0.21663(6)$	-0.2170	-0.212895
10.0	-0.12144	$-0.121353(5)$	$-0.12150(3)$	-0.1216	-0.118800
20.0	-0.06664	$-0.066639(4)$	$-0.06666(2)$	-0.06667	-0.064864
50.0	-0.02923	$-0.029276(3)$	$-0.02927(1)$		-0.028220
100.0	-0.01538	$-0.0154145(13)$	$-0.015427(4)$	-0.01535	-0.014733
160.0	-0.00988	-0.0099046			

grams. These corrections are, obviously, quite small but do improve the agreement with DMC data. For mere energy calculation, these effects are negligible, but we will see that the inclusion of triplet correlations improves the consistency between the hydrodynamic compressibility as computed from the equation of state and from the long-wavelength limit of the particle-hole interaction. More importantly, there are also quite visible improvements of the static structure functions in the vicinity of the peak region.

The ground-state energies of the two-dimensional charged-boson fluid at different densities are listed in Table IV. We found no published Monte Carlo results for that system, however, we have learned[52] about recent diffusion Monte Carlo calculations that agree with our ground-state energies typically within the same accuracy that was found in three dimensions. Our results are below the variational results by Sim, Tao, and Wu.[25] This is plausible since these authors parametrize $g(r)$ and $S(k)$ using a single parameter and then minimize the energy-expectation value with respect to this parameter, whereas we solve the full Euler equation. Furthermore, the calculation of Ref. 25 has been done in the HNC/0-approximation. Reasonable agreement is also found with the STLS results by Gold.[31]

The kinetic-energy expectation value is also a quantity of interest. For our discussion of the static response function we also need the uniform limit approximation (2.29). Our results

in 3D are shown in Fig. 1 and compared with DMC data. Again, the comparison between the full calculation and the Monte Carlo data is satisfactory, albeit the agreement is not quite as good as for the total energy, because the kinetic energy is only a fraction of the total energy ranging from 25% in the high-density limit to 5% at $r_s = 160$. The very simple uniform limit approximation is also reasonably acceptable. The results in 2D are similar and shown in Fig. 2. The two ways to calculate the kinetic energy become exact in the high-density limit

$$\lim_{r_s \to 0} \frac{T}{N} = \frac{E}{N} - \mu = \frac{P}{\rho}; \qquad (2.38)$$

it is somewhat surprising that the uniform limit approximation is also quite accurate at very low densities.

Figures 3 and 4 show the calculated pair-distribution functions $S(k)$ of the 3D and 2D systems, respectively. The long-wavelength behavior of these functions is different. In the 3D case one has $S(k) \propto k^2$, whereas in the 2D case $S(k) \propto k^{3/2}$. In the 3D case, we can again compare with Monte Carlo data. Figure 3 shows that comparison only for low densities, $r_s \geq 20$; at higher densities our results and the Monte Carlo data are indistinguishable. At lower densities, the Monte Carlo calculations show a slightly higher peak in the regime of their maxima; they are otherwise quite close.

TABLE III. Decomposition of the ground-state correlation energy E_g of the three-dimensional charged-boson fluid into HNC/0 contribution $E_{HNC/0}$ and the terms E_3 from the triplet correlations and E_e from the four- and five-body elementary diagrams.

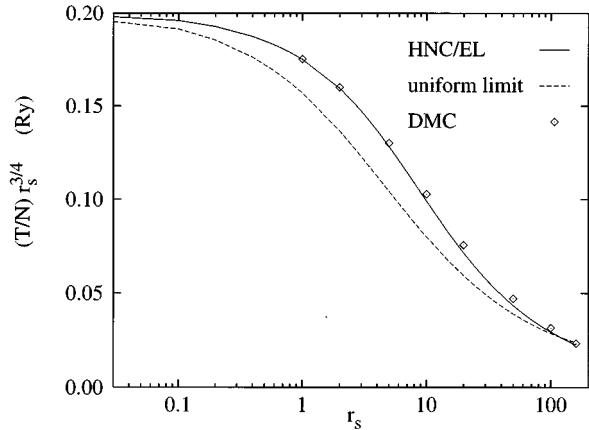| r_s	$E_{HNC/0}$	E_3	E_e	E_g (full)
0.1	-4.48794	-0.00050	-0.00011	-4.48857
1.0	-0.77578	-0.00040	-0.00058	-0.77675
2.0	-0.45091	-0.00034	-0.00079	-0.45203
5.0	-0.21540	-0.00025	-0.00093	-0.21657
10.0	-0.12045	-0.00019	-0.00080	-0.12144
20.0	-0.06596	-0.00014	-0.00055	-0.06664
50.0	-0.02890	-0.00009	-0.00024	-0.02923
100.0	-0.01520	-0.00006	-0.00012	-0.01538
160.0	-0.00976	-0.00005	-0.00007	-0.00988

FIG. 1. The kinetic energy of the charged-boson gas in 3D obtained from our calculation (solid line) is compared with the DMC data of Ref. 38. Also shown is the kinetic energy obtained in the ''uniform limit approximation'' (2.29).

TABLE IV. Ground-state energy E_g of the two-dimensional charged-boson fluid from the present calculation (including both the triplet correlations and the elementary diagrams) compared with the results by Sim, Tao, and Wu (STW) (Ref. 25) using a parametrized variational wave function, and with the results by Gold calculated using the STLS scheme (Ref. 31).

r_s	E_g (full)	STW	STLS
0.1	-5.8441		
1.0	-1.1458	-1.1062	-1.1103
2.0	-0.6740	-0.6631	-0.6484
3.0	-0.4873	-0.4818	-0.5965
4.0	-0.3844	-0.3796	
5.0	-0.3185	-0.3133	-0.3078
6.0	-0.2725	-0.2666	
8.0	-0.2122	-0.2053	
10.0	-0.1741	-0.16685	-0.1724
20.0	-0.0928	-0.086024	
50.0	-0.0394		

The only slightly unsystematic behavior is found at $r_s = 20$, where the peak of the DMC $S(k)$ is shifted inwards. At high densities the 3D and 2D structure functions are quite similar, but as the density decreases the peak of the 2D structure factor grows more rapidly. Besides the height, the peaks differ also in the position. The peaks in the 2D case are at somewhat smaller values of k.

Figures 5 and 6 show the calculated pair-distribution functions $g(r)$ of the 2D and 3D systems. The effect of screening is clearly seen in both cases: as the density increases, the pair-distribution function at zero separation, $g(0)$, approaches unity; i.e., the repulsion between the particles decreases and there is considerable overlap of charges. The results also show the screening to be weaker in the two-dimensional system. At very low densities we find a typical low-density distribution function, i.e., a large overshoot and a long-ranged oscillatory behavior. Both of these features clearly indicate the tendency of the particles to become localized as the density decreases. The peak in $g(r)$ is higher in the 2D system and the oscillations appear at a higher density than in the 3D fluid. We emphasize, however, that the
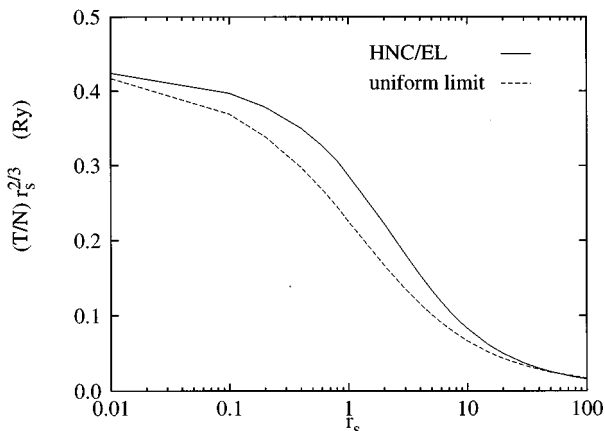
calculations presented here describe, at low densities, the overcooled fluid, not the emerging Wigner crystal.

III. DYNAMICS

A. Time-dependent correlations

A plausible way to deal with excitations within the variational approach is to allow for a time dependence of the correlation functions $u_n(\mathbf{r}_1, \ldots, \mathbf{r}_n)$. Beyond the time dependence of the components of the wave function (2.2), we must also include a time-dependent one-body function since the dynamics will normally break the translational invariance. The wave function of the excited system is again written in the Jastrow-Feenberg form

$$|\Psi(t)\rangle = \frac{e^{-iE_0 t/\hbar} e^{\frac{1}{2}\delta U(\mathbf{r}_1,\ldots,\mathbf{r}_N;t)}|\Psi_0\rangle}{[\langle\Psi_0|e^{\delta U}|\Psi_0\rangle]^{1/2}}, \qquad (3.1)$$
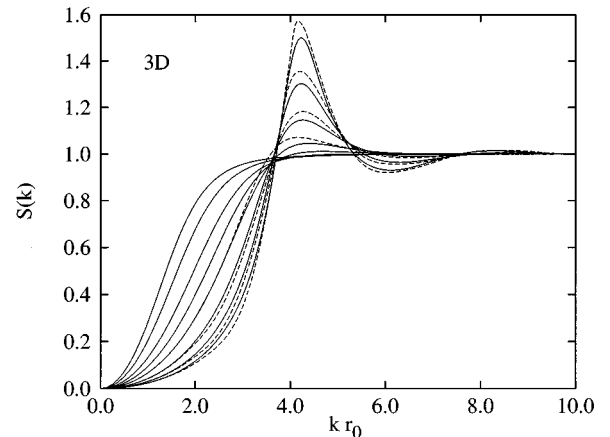

FIG. 3. The static structure function for the three-dimensional charged-boson gas for $r_s = 1$, 2, 5, 10, 20, 50, 100, and 160 (solid lines). The lines with the higher peaks correspond to the highest values of r_s. Also shown are DMC results for $r_s = 20$, 50, 100, and 160 (dashed lines, from Ref. 38).

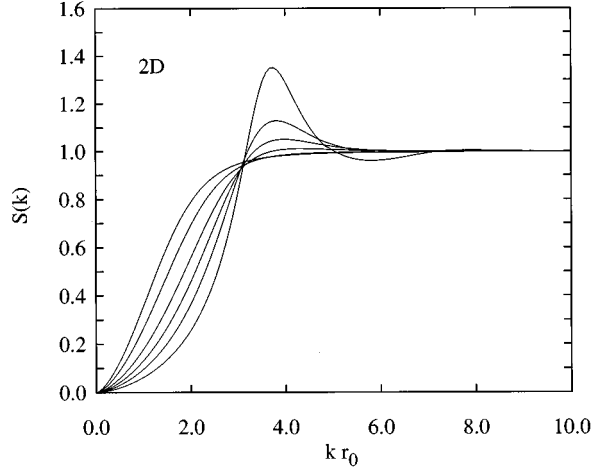FIG. 2. Same as Fig. 1 for the two-dimensional charged-boson gas.

FIG. 4. The static structure function for the two-dimensional charged-boson gas for $r_s = 1, 2, 5, 10, 20,$ and 50. The lines with the higher peaks correspond to the higher values of r_s.

where $|\Psi_0\rangle$ is the (variational) ground state, and

$$\delta U(\mathbf{r}_1, \ldots, \mathbf{r}_N; t) = \sum_i \delta u_1(\mathbf{r}_i; t) + \sum_{i<j} \delta u_2(\mathbf{r}_i, \mathbf{r}_j; t) \tag{3.2}$$

is a time-dependent complex function representing fluctuations of the correlation functions. Since the excitations can be considered as small perturbations of the ground state, one can treat δU to the leading nontrivial order.

Restricting the time dependence to the *one-body component only* leads directly to the Feynman theory of excitations[53] and to the dispersion relation (2.22). It provides an upper bound for the lowest-lying excitation and is exact in the long-wavelength limit, but has deficiencies at shorter wavelengths. The cause of this deficiency is evident from the variational point of view: When the wavelength of an excitation becomes comparable to the average particle distance, one should expect that all correlations that are important at that wavelength are also time dependent. Consequently, it was found in liquid ^{4}He (Refs. 54–58) that much of the energetics of the excitations in the medium to high momentum range can be attributed to fluctuating short-ranged correlations, and the same is expected to be true in the boson plasma. For the implementation of the present theory of excitations and dynamic structure the structure function $S(k)$ is the essential input. This $S(k)$ is provided by our ground-state calculations described above, but it may equally well be taken from other calculations.

The time-dependent correlations are determined by the action principle

$$\delta J = \delta \int_{t_1}^{t_2} \mathcal{L}[\Psi(t), \dot{\Psi}(t)] dt = 0 \tag{3.3}$$

with the Lagrangian

$$\mathcal{L} = \left\langle \Psi(t) \left| H - i\hbar \frac{\partial}{\partial t} \right| \Psi(t) \right\rangle = \left\langle \Psi_0 \left| H - E_0 - i\hbar \frac{\partial}{\partial t} \right| \Psi_0 \right\rangle. \tag{3.4}$$
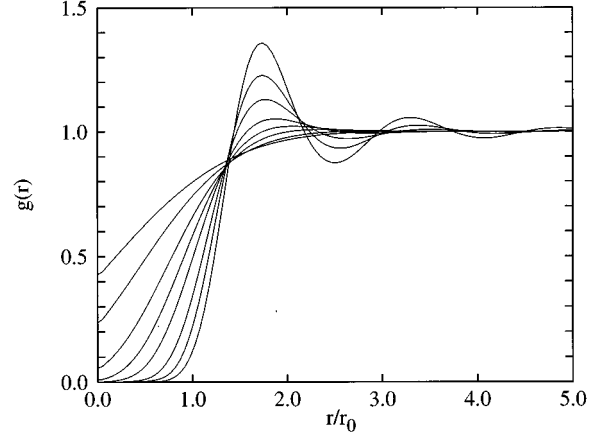

FIG. 5. The pair-distribution function for the three-dimensional charged-boson gas for $r_s = 1, 2, 5, 10, 20, 50, 100,$ and 160. The lines with the higher peaks correspond to the higher values of r_s.

The stationarity principle (3.3) leads to four Euler-Lagrange equations for the real and imaginary parts of δu_1 and δu_2, which are conveniently written in the form of two continuity equations,

$$\nabla_1 \cdot \mathbf{j}_1(\mathbf{r}_1; t) = \dot{\rho}_1(\mathbf{r}_1; t),$$
$$\nabla_1 \cdot \mathbf{j}_2(\mathbf{r}_1, \mathbf{r}_2; t) + (1 \leftrightarrow 2) = \dot{\rho}_2(\mathbf{r}_1, \mathbf{r}_2; t) \tag{3.5}$$

with the one- and two-particle currents

$$-i\mathbf{j}_1(\mathbf{r}_1; t) = \frac{\hbar}{2m} \left\{ \bar{\rho}_1(\mathbf{r}_1) \nabla_1 \delta u_1(\mathbf{r}_1; t) \right.$$
$$\left. + \int d\mathbf{r}_2 \bar{\rho}_2(\mathbf{r}_1, \mathbf{r}_2) \nabla_1 \delta u_2(\mathbf{r}_1, \mathbf{r}_2; t) \right\},$$

$$-i\mathbf{j}_2(\mathbf{r}_1, \mathbf{r}_2; t) = \frac{\hbar}{2m} \left\{ \bar{\rho}_2(\mathbf{r}_1, \mathbf{r}_2) [\nabla_1 \delta u_1(\mathbf{r}_1; t) \right.$$
$$+ \nabla_1 \delta u_2(\mathbf{r}_1, \mathbf{r}_2; t)]$$
$$\left. + \int d\mathbf{r}_3 \bar{\rho}_3(\mathbf{r}_1, \mathbf{r}_2, \mathbf{r}_3) \nabla_1 \delta u_2(\mathbf{r}_1, \mathbf{r}_3; t) \right\}, \tag{3.6}$$
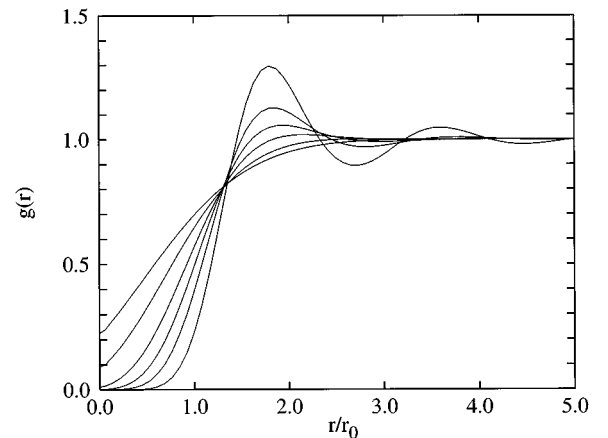

FIG. 6. The pair-distribution function for the two-dimensional charged-boson gas for $r_s = 1, 2, 5, 10, 20,$ and 50. The lines with the higher peaks correspond to the higher values of r_s.

where $\overline{\rho}_1$ and $\overline{\rho}_2$ are the time-independent ground-state quantities. The derivatives of the correlation functions are related to the derivatives of the pair-distribution functions through the set of exact BGY equations.[43]

Since the relationships between the time-dependent components of the pair-correlation and pair-distribution functions involve ground-state densities up to four-body distribution function ρ_4, approximations are necessary, and different implementations use different approximations depending on the problems under consideration, and on the system investigated.

B. Dynamic response function

A convenient and mathematically transparent level at which one can deal with fluctuating pair correlations is the uniform limit approximation for the kernels of the equations of motion (3.5) and (3.6). The underlying assumptions have already been mentioned in connection with Eq. (2.27). In a somewhat different derivation of the dynamics, this approximation has also been used by Campbell *et al.*[59,54] to calculate the phonon-roton spectrum in liquid ^{4}He; the equations-of-motion method has first been used in Ref. 55, the connection to the derivations of Campbell[54] and Jackson[60–62] has, in the somewhat more general case of an inhomogeneous system, been derived in Refs. 58 and 63. Important formal properties of the dynamic structure function have been discussed by Jackson;[60–62] the resulting formalism is flexible enough to be used also in inhomogeneous geometries.[58,63] The theory leads to a dynamic response function of the plausible form

$$\chi(k,\omega) = \frac{S(k)}{\hbar\omega - \varepsilon(k) - \Sigma(k,\omega)} + \frac{S(k)}{-\hbar\omega - \varepsilon(k) - \Sigma(k,-\omega)}, \tag{3.7}$$

where $S(k)$ is the static structure function, $\varepsilon(k)$ the Feynman excitation spectrum (2.22) and $\Sigma(k,\omega)$ is the plasmon/phonon self-energy arising from phonon-splitting and recombination processes. In the zero-frequency limit we obtain the static response function

$$\chi^{CBF}(k,0) = -\frac{2S(k)}{\varepsilon(k) + \Sigma^{CBF}(k,0)}. \tag{3.8}$$

If we ignore the self-energy correction $\Sigma(k,\omega)$, the response function (3.7) reduces to the familiar response function in the random phase approximation

$$\chi^{RPA}(k,\omega) = \frac{2t(k)}{\hbar^2\omega^2 - \varepsilon^2(k)} = \frac{\chi_0(k,\omega)}{1 - \widetilde{V}_{p\text{-}h}(k)\chi_0(k,\omega)} \tag{3.9}$$

with the response function of the noninteracting boson system

$$\chi_0(k,\omega) = \frac{2t(k)}{\hbar^2\omega^2 - t^2(k)}. \tag{3.10}$$

The $\widetilde{V}_{p\text{-}h}(k)$ is the ''particle-hole interaction'' introduced in Eq. (2.17) in the optimization problem of the ground state; in fact the result (3.9) is not surprising since the static structure function $S(k)$ given in Eq. (2.16) is readily identified with the random phase approximation for $S(k)$ for a given, static interaction $\widetilde{V}_{p\text{-}h}(k)$. In this approximation, the only excitation is one collective mode with the Feynman dispersion relation $\varepsilon(k)$.

In the usual implementations of the formalism (3.7) the self-energy correction has the form

$$\Sigma^{CBF}(k,\omega) = \frac{1}{2}\int \frac{d^dp\,d^dq}{(2\pi)^d\rho}\,\delta(\mathbf{k}+\mathbf{p}+\mathbf{q})\frac{|V_3(\mathbf{k};\mathbf{p},\mathbf{q})|^2}{\hbar\omega - \varepsilon(p) - \varepsilon(q)}, \tag{3.11}$$

where the three-plasmon/phonon coupling matrix element is given in terms of ground-state quantities as[54]

$$V_3(\mathbf{k};\mathbf{p},\mathbf{q}) = \frac{\hbar^2}{2m}\sqrt{\frac{S(p)S(q)}{S(k)}}[\mathbf{k}\cdot\mathbf{p}\widetilde{X}(p) + \mathbf{k}\cdot\mathbf{q}\widetilde{X}(q) - k^2\widetilde{u}_3(\mathbf{k},\mathbf{p},\mathbf{q})]. \tag{3.12}$$

The irreducible three-body vertex $\widetilde{u}_3(\mathbf{k},\mathbf{p},\mathbf{q})$ has been defined in Eq. (2.23). It is important to keep this term since it accounts for the qualitatively correct density dependence of the roton minimum.[54] Correction terms to the three-body vertex (3.12) beyond the approximation used here have been found to be small.[41] Improvements of the theory of excitations would involve more self-consistent treatments of the energy denominator and possibly four-body vertices. We shall refer to the choice (3.11), (3.12) of the self-energy as to the CBF approximation for the self-energy, and to the corresponding response function as $\chi^{CBF}(k,\omega)$.

It is straightforward to determine both the long- and the short-wavelength limits of the self-energy and, hence, the static response function. For *short wavelengths*, $k\to\infty$, we find

$$\lim_{k\to\infty}\Sigma^{CBF}(k,0) = -\frac{\hbar^2}{2m}\int\frac{d^dq}{(2\pi)^d\rho}(\hat{\mathbf{k}}\cdot\hat{\mathbf{q}})^2 q^2\widetilde{X}^2(q)S(q) = \begin{cases} -\dfrac{4}{3}\dfrac{T_{RPA}}{N} & \text{(in 3D)} \\[2ex] -2\dfrac{T_{RPA}}{N} & \text{(in 2D)}. \end{cases} \tag{3.13}$$

The fact that we obtain only the ''uniform limit approximation'' of the kinetic energy is, of course, due to our approximations for the three-body vertex function. In a more complete theory one should expect to obtain here the full kinetic-energy expectation value.

In the long-wavelength limit of the self-energy, on the other hand, one obtains

$$\Sigma^{CBF}(k,\omega) \sim \frac{1}{2}\varepsilon(k)t(k)\int\frac{d^dq}{(2\pi)^d\rho}\left(\frac{\varepsilon(q)}{\hbar\omega_{pl} + 2\varepsilon(q)}\right)^2\frac{(S^2(q) - 1 + 2(\hat{k}\cdot\hat{q})^2[q/S(q)]dS(q)/dq)^2}{\hbar\omega - 2\varepsilon(q)}, \quad \text{as } k\to 0+. \tag{3.14}$$

We have written the result in a somewhat more general form than necessary for the present purpose since the above expression is also needed to calculate the plasmon dispersion coefficient. In three dimensions, the limit $\lim_{k\to 0}\varepsilon(k)=\hbar\omega_{\text{pl}}$ defines the plasmon energy. In two dimensions $\hbar\omega_{\text{pl}}=0$, because in the long-wavelength limit the collective excitation energy goes to zero like $\sqrt{k}$. Thus, both the long-wavelength limit of the static response function and—as we shall see—the plasmon dispersion relation are modified in three dimensions by the self-energy correction, whereas they are unaffected in two dimensions. The result (3.14) is essential to complete our proof of the consistency between the hydrodynamic compressibility and the long-wavelength limit of the static response function at high densities.

C. Compressibility

The hydrodynamic compressibility is related to the long-wavelength limit of the static response function

$$\lim_{k\to 0}\chi^{-1}(k,0)=-\frac{1}{\rho K_T}-\widetilde{v}(k). \tag{3.15}$$

In the case of the charged fluids the compressibility measures the response of the system to a screened external charge[64]; that is why the singular Coulomb potential is subtracted from the definition.

The expression for the static response function (3.8) gives two contributions to the compressibility. We define the variational incompressibility as

$$\frac{1}{\rho K_T^{\text{var}}}\equiv \lim_{k\to 0+}[\widetilde{V}_{p\text{-}h}(k)-\widetilde{v}(k)] \tag{3.16}$$

and the full, self-energy corrected compressibility as

$$\frac{1}{\rho K_T}=\frac{1}{\rho K_T^{\text{var}}}+\lim_{k\to 0+}\frac{\Sigma^{\text{CBF}}(k,0+)}{2S(k)}. \tag{3.17}$$

The above microscopic definition of the compressibility does generally not agree with the hydrodynamic compressibility defined in Eq. (2.19) for any diagram-based microscopic theory, unless it is exact. This inconsistency has been studied very carefully in ^{4}He and was found to be inconsequential for the energetics and affecting only very long-wavelength behaviors of the particle-hole interaction and the

structure function.[65] One would expect the same to be true in the present case. One may take advantage of such understood inconsistencies and calculate the same quantity in different ways as a test for the legitimacy of diagrammatical or numerical approximations.

It is then of interest to study the high-density limit where exact expressions for both the hydrodynamic and microscopic compressibilities can be derived. We get the hydrodynamic compressibilities in three and two dimensions using Eqs. (2.34)–(2.37),

$$\frac{1}{\rho K_T}=\frac{1}{4}\mu=-0.25096r_s^{-3/4}\ \text{Ry}\quad(\text{in 3D}),$$

$$\tag{3.18}$$

$$\frac{1}{\rho K_T}=\frac{1}{3}\mu=-0.57491r_s^{-2/3}\ \text{Ry}\quad(\text{in 2D}).$$

The leading order in r_s of the microscopic incompressibility in the high-density limit can be evaluated using the uniform limit approximation (2.27) and the structure function given in Eq. (2.33). The main contribution comes from the particle-hole potential calculated within the HNC/0 approximation,

$$\frac{1}{\rho K_T^{\text{HNC}}}=-\frac{1}{3\pi}r_s^{-3/4}\int_0^\infty d\xi\,\xi^4[S(\xi)-1]^2$$

$$=-0.222912r_s^{-3/4}\quad(\text{in 3D}), \tag{3.19}$$

$$\frac{1}{\rho K_T^{\text{HNC}}}=-\frac{1}{4}r_s^{-2/3}\int_0^\infty d\xi\,\xi^3[S(\xi)-1]^2$$

$$=-0.524999r_s^{-2/3}\ (\text{in 2D}). \tag{3.20}$$

There is a 10% discrepancy between these results and the exact hydrodynamic compressibilities (3.18).

In two dimensions the only correction of the order of $r_s^{-2/3}$ comes from the triplet correlations in the particle-hole interaction defined in Eq. (2.26),

$$\Delta\widetilde{V}_{p\text{-}h}^{(3)}(0+)=-\frac{1}{16}r_s^{-2/3}\int_0^\infty d\xi\frac{\xi^3}{S(\xi)}[S(\xi)-1]^4. \tag{3.21}$$

By adding this to the HNC/0 contribution one recovers the exact result $1/(\rho K_T^{\text{var}})=\mu/3$.

In the three-dimensional case an additional correction enters into the triplet-correlation contribution due to the existence of a plasmon mode,

$$\Delta\widetilde{V}_{p\text{-}h}^{(3)}(0+)=-\frac{1}{12\pi}r_s^{-3/4}\int_0^\infty d\xi\frac{\xi^4}{S(\xi)}\left\{[S(\xi)-1]^4-\left(\frac{\hbar\omega_{\text{pl}}}{\hbar\omega_{\text{pl}}+2\varepsilon(\xi)}\right)^2\left[[S^2(\xi)-1]^2+\frac{4}{3}[S^2(\xi)-1]\frac{\xi}{S(\xi)}\frac{dS(\xi)}{d\xi}\right.\right.$$

$$\left.\left.+\frac{4}{5}\left(\frac{\xi}{S(\xi)}\frac{dS(\xi)}{d\xi}\right)^2\right]\right\}. \tag{3.22}$$

The term proportional to the plasmon frequency is exactly canceled by the self-energy contribution from Eq. (3.14). Similar to the two-dimensional case, we are left with an expression

$$\Delta \widetilde{V}_{p\text{-}h}^{(3)}(0+) + \lim_{k \to 0+} \frac{\Sigma^{\text{CBF}}(k,0)}{2S(k)} = -\frac{1}{12\pi} r_s^{-3/4} \int_0^\infty d\xi \frac{\xi^4}{S(\xi)} [S(\xi) - 1]^4. \tag{3.23}$$

This, together with HNC/0 contribution, gives the exact compressibility also in three dimensions. We have recovered an interesting result that, due to the finite long-wavelength limit of the excitations, both the triplet correlations *and* self-energy corrections are needed to obtain consistency between the hydrodynamic and microscopic compressibilities to leading order in the high-density expansion, whereas in two dimensions triplet correlations alone are sufficient, and the self-energy gives no correction.

The compressibility of the charged-boson fluid is negative over the whole density regime, the ground-state energy being entirely due to correlations. The same applies for the pressure. While we have shown above that, when both triplet correlations and self-energy corrections are included, the microscopic and the hydrodynamic compressibility agree *in the high-density limit*, this is normally not true at finite densities. Figure 7 shows our results for the inverse compressibility in 3D from different calculations. The inverse compressibility obtained by differentiating the equation of state agrees with the Monte Carlo data; this is expected due to the good agreement of the energies, and any discrepancies are due to differences in the fitting procedure, but not generic. The situation is different for the microscopically derived incompressibility. In Fig. 7 we show separately the variational and self-energy contributions. At high densities the self-energy corrections significantly improve the variational estimate, consistently with the above proof that the exact value is reproduced in the high-density limit. At lower densities, the microscopic definition overestimates the inverse compressibility by about 20%; this is somewhat less than what has been found in ^{4}He. We attribute this mismatch essentially to the limited set of elementary diagrams calculated here; justification for that is provided by the comparison with the two-dimensional charged-boson gas (Fig. 8) and with ^{4}He in both two and three dimensions, where the self-energy corrections are zero.

D. Static response and local-field factor

Properties of electronic systems have historically often been discussed in terms of a "local-field factor," which describes the short-range structure of the system. (For a review, see, for example, Ref. 66). Generally, one writes the exact response function as

$$\chi(k,\omega) = \frac{\chi_0(k,\omega)}{1 - \widetilde{v}(k)[1 - G(k,\omega)]\chi_0(k,\omega)}, \tag{3.24}$$

and tries to derive properties of $G(k,\omega)$. While the formulation (3.24) is, in principle, completely general, it conveys the notion that the analytic structure of the field factor is somehow simpler than that of the full response function, and in particular that the analytic structure of the response function is to some extent dominated by $\chi_0(k,\omega)$. By comparing the

response functions obtained from Eqs. (3.7) and (3.24) we shall see that this is not true for large parts of the spectrum.

The literature on properties of the local-field factor is vast and occasionally controversial, to a large extent due to incompatible definitions. The identification of the effective interaction $\widetilde{V}_{p\text{-}h}(k)$ with the particle-hole interaction of the RPA in Eq. (3.9) suggests an immediate connection to the *static* local-field factor through[67–71]

$$\widetilde{V}_{p\text{-}h}(k) = \widetilde{v}(k)[1 - G^{\text{RPA}}(k)]. \tag{3.25}$$

$\widetilde{V}_{p\text{-}h}(k)$ is, on the other hand, related to the static structure function $S(k)$ through the Bogoliubov relation (2.16). A bosonic system allows here for a particularly simple representation,

$$1 - G^{\text{RPA}}(k) = \frac{\hbar^2 k^2}{4m\widetilde{v}(k)} [S^{-2}(k) - 1]. \tag{3.26}$$

This is *one way* to define a static local-field factor; it has a certain appeal simply because it allows for a one-to-one connection with the static structure function, which is known today for a large number of systems from either experiments, accurate microscopic calculations, or simulations. We note, however, that the momentum-space factorization in the form (3.24) or (3.25) is rather artificial: microscopic many-body theories would rather suggest a factorization in coordinate space; cf. Eq. (2.17). Such a coordinate space formulation of local screening is more appropriate since it is also applicable if the bare interparticle interaction has a hard core or in situations with broken spatial symmetry.

Another way to define the static local-field factor is from the *static* response function $\chi(k,0)$,

$$\widetilde{v}(k)[1 - G(k,0)] = -\frac{1}{2}t(k) - \frac{1}{\chi(k,0)} \equiv \widetilde{v}(k)[1 - G^{\text{stat}}(k)]. \tag{3.27}$$

Evidently, there is no *a priori* reason that the static local-field factor defined in this manner should agree with $G^{\text{RPA}}(k)$ defined above; in fact they agree — by definition — only in the random phase approximation $\Sigma(k,0) = 0$.

Using Eqs. (2.16), (3.25), and (3.27) we get

$$\widetilde{v}(k)[1 - G^{\text{stat}}(k)] = \widetilde{v}(k)[1 - G^{\text{RPA}}(k)] + \frac{\Sigma^{\text{CBF}}(k,0)}{2S(k)} \tag{3.28}$$

or

$$G^{\text{stat}}(k) = G^{\text{RPA}}(k) - \frac{\Sigma^{\text{CBF}}(k,0)}{2S(k)\widetilde{v}(k)}. \tag{3.29}$$

Properties of $G^{\text{stat}}(k)$ have been discussed by Holas,[66] and it is worth verifying that the response function (3.7) with the self-energy (3.11) is consistent with the properties of $G^{\text{stat}}(k)$ derived there. Inserting the asymptotic limits (3.13)
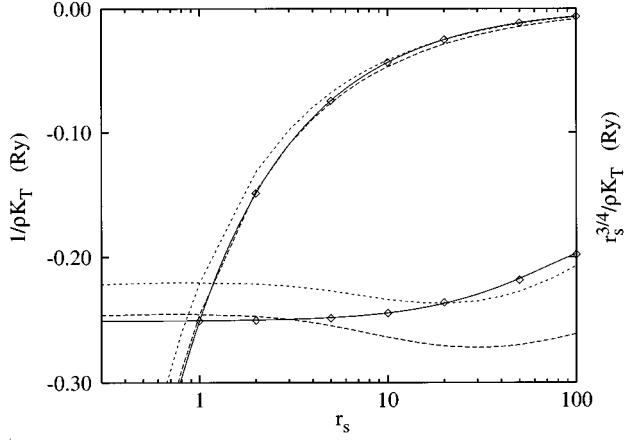
FIG. 7. The inverse compressibility $1/\rho K_T$ of the charged-boson gas in three dimensions is shown as obtained from our calculation by differentiating the equation of state (solid line), from the long-wavelength limit of the static interaction, [Eq. (3.16), short-dashed line], and with the inclusion of self-energy corrections [Eq. (3.17), long-dashed line]. Also shown are the Monte Carlo data of Ref. 38 (diamonds). The lower three curves and the scale at the right margin refer to the same data, scaled by a factor $r_s^{3/4}$.

into Eq. (3.29), the result can be cast into an asymptotic expression for the static local-field factor $G^{\text{stat}}(k)$ in the form[66,38]

$$G^{\text{stat}}(k) \sim \frac{2}{3}\frac{T_{\text{RPA}}}{N}\frac{k^2}{4\pi e^2 \rho} \quad \text{(in 3D as } k\to\infty\text{)}, \qquad (3.30)$$

$$G^{\text{stat}}(k) \sim \frac{T_{\text{RPA}}}{N}\frac{k}{2\pi e^2 \rho} \quad \text{(in 2D as } k\to\infty\text{)}. \qquad (3.31)$$

Thus, our theory is, within the approximation chosen for the three-body vertex, consistent with the known asymptotic limits. The results (3.30) and (3.31) are not new, but their verification in the present context serves as a demonstration of at what order of our theory this asymptotic limit is obtained, and as an assessment of the accuracy of the predictions one should expect for that limit. The analysis could also
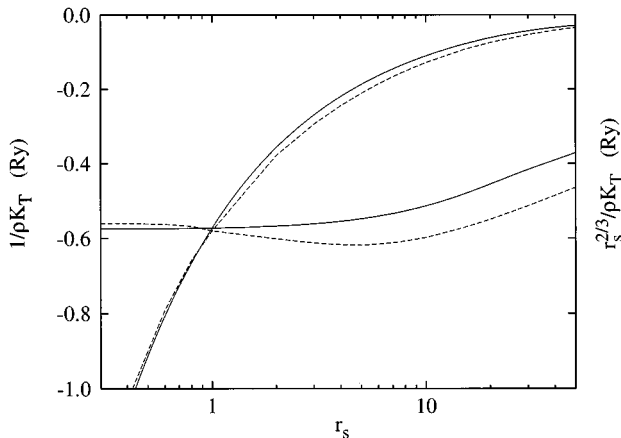

FIG. 8. Same as Fig. 7 for the two-dimensional charged-boson gas. The lower two curves and the scale at the right margin refer to the same data, scaled by a factor $r_s^{2/3}$.
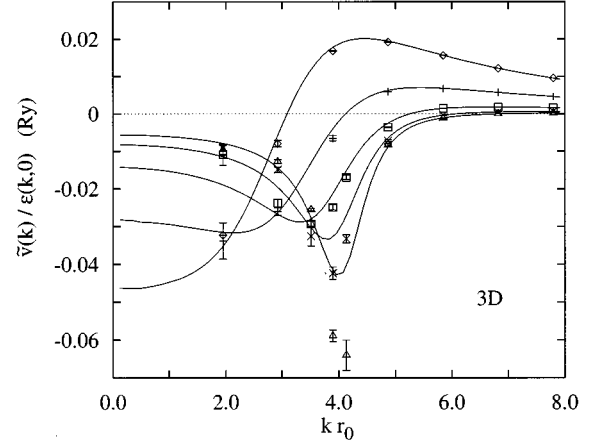

FIG. 9. The static effective interaction $\widetilde{v}(k)/\epsilon(k,0)$ is shown for the 3D charged-boson gas at $r_s = 10,\ 20,\ 50,\ 100,$ and 160 as calculated from CBF theory (solid lines). The function with the lowest value at the origin corresponds to the lowest value of r_s. Also shown are DMC results of Ref. 38 (symbols with error bars). Different symbols denote different r_s values [$r_s=10$ (diamonds), 20 (plusses), 50 (squares), 100 (crosses), and 160 (triangles)].

provide some guidance towards developing more complete forms for the three-body vertex function. For further discussion, we are satisfied with the observation that the approximation (2.29) appears to be reasonable.

Before turning to the comparison of various static local-field factors, we first calculate the static dielectric function

$$\epsilon(k,0) = \frac{1}{1+\widetilde{v}(k)\chi(k,0)}, \qquad (3.32)$$

and the static effective interaction $\widetilde{v}(k)/\epsilon(k,0)$ which describes how a test charge of unit strength interacts with the system.[64] We believe that these are in general the more appropriate quantities to discuss since there are well-defined operational procedures to obtain these functions from experiments or simulations, whereas "field corrections" are auxiliary quantities representing (approximations for) certain sets of Feynman diagrams. Figures 9 and 10 show our results for the static effective interaction using the full CBF static response function (3.8) for three and two dimensions. In three dimensions comparison with Monte Carlo results is again possible. The long-wavelength limit of the effective interaction is determined by the compressibility

$$\lim_{k\to 0+} \frac{\widetilde{v}(k)}{\epsilon(k,0)} = \frac{1}{\rho K_T}, \qquad (3.33)$$

and is thus negative. In the short wavelengths it behaves like the bare Coulomb potential. Up to $r_s=50$, our results agree very well with the DMC results.[38] At larger r_s a clear minimum begins to form near $kr_0=4$ and our results underestimate the depth of that minimum. In two dimensions we have plotted a wider range of r_s values from $r_s=1$ to 50. The general behavior is very similar to the three-dimensional case, but it is worth noting that the minimum, located at $kr_0=3.4$, is already at $r_s=50$ fifteen times deeper than in the three-dimensional case, suggesting that the density wave in-
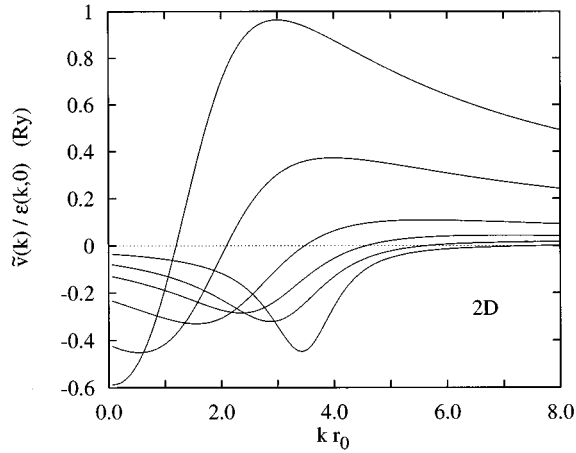
FIG. 10. The static effective interaction $\tilde{v}(k)/\epsilon(k,0)$ is shown for the 2D charged-boson gas at $r_s = 1, 2, 5, 10, 20$, and 50 as calculated from CBF theory. The function with the lowest value at the origin corresponds to the lowest value of r_s.

stability or the Wigner crystallization occurs in two dimensions at much higher densities.

Figure 11 shows the *static* local-field factor $G^{\text{stat}}(k)$ in 3D and compares it with the Monte Carlo data of Ref. 38. The Monte Carlo data used to calculate $G^{\text{stat}}(k)$ is the same as for the static effective interaction, because these quantities are related by known functions,

$$G^{\text{stat}}(k) = \frac{1}{1 - \epsilon(k,0)} - \frac{1}{\tilde{v}(k)\chi_0(k,0)}. \qquad (3.34)$$

In this case the comparison focuses more on the high momentum transfers, which is enhanced by a factor k^4 from the static effective interaction. The main mismatch is found at $r_s = 10$ when $kr_0 > 5$. Some of this inaccuracy can be related to the asymptotic value (3.30) calculated in the uniform limit approximation; cf. Fig. 1. At higher r_s values our results agree very well with the Monte Carlo data for the whole
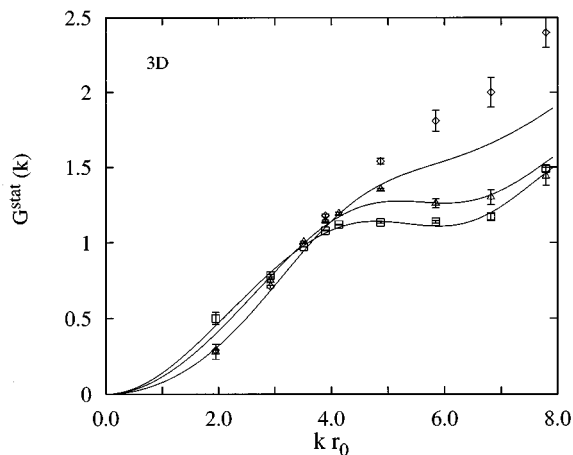

FIG. 11. The static local-field factor $G^{\text{stat}}(k)$ is shown, for $r_s = 10, 50$, and 160, as obtained from our calculation (solid lines) and from the DMC calculation of Ref. 38 (symbols with error bars). The curves with the largest asymptotic values correspond to the smallest value of r_s.
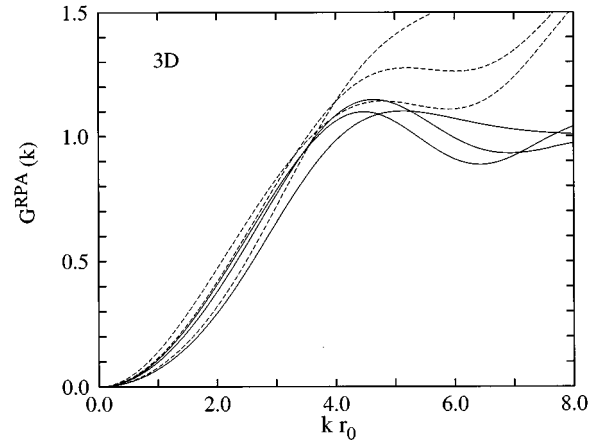

FIG. 12. The RPA static local-field factor $G^{\text{RPA}}(k)$ is shown, in 3D, for $r_s = 10, 50$, and 160 (solid lines). Also shown are, for comparison, the functions $G^{\text{stat}}(k)$ at the same densities (dashed lines). The curves with the largest asymptotic values correspond to the smallest value of r_s.

momentum range. Figures 12 and 13 finally show a comparison between $G^{\text{RPA}}(k)$ and $G^{\text{stat}}(k)$ in both two and three dimensions. As expected, these local-field factors agree for long and medium wavelengths typically up to $kr_0 = 4$.

E. Analytic structure of the response function

Before we proceed with applications of the dynamic correlation theory, we derive a number of analytic properties of the response function (3.7) related to sum rules and to the existence of collective modes. The dynamic response function is linked, through sum rules, to ground-state properties. Primarily, we have in mind the static structure function $S(k)$, which can be calculated with high accuracy without ever mentioning excitations. $S(k)$ is related to the response function through
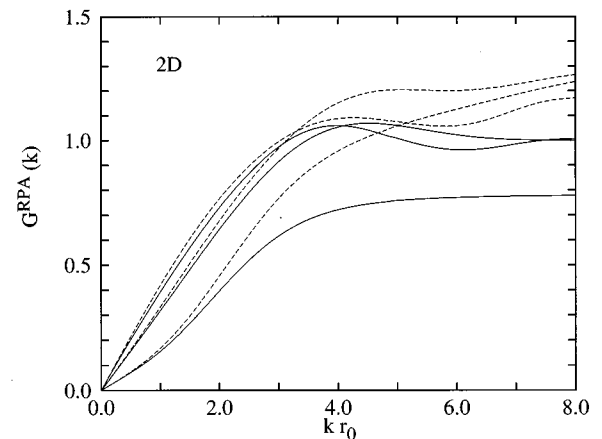

FIG. 13. The RPA static field corrections $G^{\text{RPA}}(k)$ are shown, in 2D, for $r_s = 1, 10$, and 50 (solid lines). Also shown are, for comparison, the functions $G^{\text{stat}}(k)$ at the same densities (dashed lines). The $G^{\text{stat}}(k)$ curves with the largest asymptotic values correspond to the smallest value of r_s; both local field corrections agree for long wavelengths.

$$S(k) = \int_{-\infty}^{\infty} \frac{d\hbar\omega}{2\pi} \text{Im } \chi(k,\omega). \qquad (3.35)$$

Historically, models for the response function have often been used to calculate $S(k)$. An attractive alternative that takes into account the progress made in ground-state theories is to use static structure functions obtained from accurate ground-state calculations to determine properties of the response function. For example, the Feynman approximation can be constructed by requiring that the frequency integral is exhausted by a single pole, and that the static structure function is reproduced from the RPA response function (3.9) by definition of the effective interaction. This *defines* the RPA local-field correction $G^{\text{RPA}}(k)$, see Eq. (3.25).

However, the Feynman theory is, as we have pointed out repeatedly, not very accurate when the wavelength of the excitation is comparable to the interparticle distance. On the other hand, according to our strategy outlined above, any improved theory of $\chi(k,\omega)$ should reproduce the known $S(k)$. Precisely this feature of the CBF excitation theory was proven by Jackson:[62] The self-energy correction $\Sigma(k,\omega)$ does not affect the first two of the moment sum rules in the sense that the moments of the response function (3.7) are identical to those of the Feynman response function

$$S(k) = \int_{-\infty}^{\infty} \frac{d\hbar\omega}{2\pi} \text{Im } \chi^{\text{RPA}}(k,\omega) = \int_{-\infty}^{\infty} \frac{d\hbar\omega}{2\pi} \text{Im } \chi^{\text{CBF}}(k,\omega),$$

$$(3.36)$$

$$\frac{\hbar^2 k^2}{2m} = \int_{-\infty}^{\infty} \frac{d\hbar\omega}{2\pi} \hbar\omega \text{Im } \chi^{\text{RPA}}(k,\omega)$$

$$= \int_{-\infty}^{\infty} \frac{d\hbar\omega}{2\pi} \hbar\omega \text{Im } \chi^{\text{CBF}}(k,\omega).$$

In other words, the self-energy correction changes the relative weight of the individual excitations and resonances, but it does not change the integrated strength.

The collective modes of the system are found by determining the poles (note that all poles are on the real axis[62]) of the response function (3.7), in other words, by solving the implicit equation

$$\hbar\omega_0(k) = \varepsilon(k) + \Sigma(k,\omega_0(k)). \qquad (3.37)$$

The strength of the collective mode is given by

$$Z(k) = S(k) \left[1 - \frac{\partial}{\partial\omega}\Sigma(k,\omega) \Big|_{\omega = \omega_0(k)} \right]^{-1}. \qquad (3.38)$$

From our definition (3.11) of the self-energy follows the inequality

$$\Sigma^{\text{CBF}}(k,\omega) \leq \Sigma^{\text{CBF}}(k,0) \leq 0 \qquad (3.39)$$

from which one immediately sees that the lowest collective mode satisfies the exact inequality[72]

$$\hbar\omega_0(k) \leq -\frac{2S(k)}{\chi^{\text{CBF}}(k,0)}. \qquad (3.40)$$

While it is reassuring that our microscopic approach satisfies known exact sum rules and inequalities as a consequence of its structure, we will see momentarily that the inequality (3.40) is of rather limited use in determining features of either the excitation spectrum, or the static response function. The reason is that it gives information *neither* on the pole strength $Z(k)$, *nor* on the existence of stable collective modes. We shall encounter examples of both: a case where the pole strength of the lowest collective mode is infinitesimal, and a case where no real collective mode exists. The latter example is in fact a well-known consequence of anomalous dispersion.

In writing down Eq. (3.37) we have to assume that $\Sigma(k,\omega_0(k))$ is real. This is the case when the energy denominator in Eq. (3.11) does not change sign, which is true when the collective energy is *below* the critical value

$$\hbar\omega_0 < \hbar\omega_{\text{crit}}(k) \equiv \min_{\mathbf{q}}[\varepsilon(q) + \varepsilon(|\mathbf{k}+\mathbf{q}|)] \qquad (3.41)$$

determining the continuum boundary. Above that energy, the self-energy is complex. Moreover, for $\hbar\omega < \hbar\omega_{\text{crit}}(k)$, it follows from Eq. (3.11) that

$$\frac{d\Sigma(k,\omega)}{d\omega} < 0 \quad \text{for} \quad \hbar\omega < \hbar\omega_{\text{crit}}(k). \qquad (3.42)$$

In order to determine if Eq. (3.37) has a solution, we must find out whether $\Sigma(k,\omega)$ becomes singular at the branch cut $\omega = \omega_{\text{crit}}(k)$ or not. This depends, of course, on the details of the reference spectrum in the energy denominator of Eq. (3.37). We shall study here two relevant cases.

The first case is that the reference spectrum $\varepsilon(k)$ is convex. This refers typically to the regime of high momentum transfer where the spectrum approaches the single-particle kinetic energy; the reader is referred to the discussion of the dynamic structure for examples. When $\hbar\omega_{\text{crit}}(k) = 2\varepsilon(k/2) < \varepsilon(k)$, this critical energy is *below* the reference energy. In order to determine whether Eq. (3.37) has a solution, we must therefore study the analytic behavior of $\Sigma(k,\omega)$ as a function of ω near the branch point $\omega = \omega_{\text{crit}}(k)$. We shall treat only the simplest cases here, assuming a monotonically growing, convex spectrum $\varepsilon'(k/2) > 0$ and $\varepsilon''(k/2) > 0$ and we are interested in the singular behavior only. The case of the two-dimensional system has been dealt with in Ref. 58;` the three-dimensional case follows essentially the same lines. The result is

$$\lim_{\hbar\omega \to 2\varepsilon(k/2)} \Sigma^{\text{CBF}}(k,\omega) = -\frac{|V_3(\mathbf{k}; -\mathbf{k}/2, -\mathbf{k}/2)|^2}{8\pi\rho} \frac{k\sqrt{2\varepsilon(k/2) - \hbar\omega}}{2\varepsilon'(k/2)\sqrt{\varepsilon''(k/2)}} \quad \text{(in 3D)}, \qquad (3.43)$$

$$\lim_{\hbar\omega \to 2\varepsilon(k/2)} \Sigma^{\text{CBF}}(k,\omega) = \frac{|V_3(\mathbf{k}; -\mathbf{k}/2, -\mathbf{k}/2)|^2}{4\pi\rho} \frac{\ln(2\varepsilon(k/2) - \hbar\omega)}{\sqrt{2\varepsilon'(k/2)\varepsilon''(k/2)/k}} \quad \text{(in 2D)}. \qquad (3.44)$$

The comparison between the two- and the three-dimensional cases is quite interesting. The self-energy is monotonically decreasing [cf. Eq. (3.42)] and has in two dimensions a logarithmic singularity at the branch point, which guarantees that the dispersion relation (3.37) always has a real solution below the Feynman spectrum. In three dimensions, however, the self-energy remains *finite* at the branch cut and, hence, the existence of a discrete collective excitation can no longer be guaranteed.

The second relevant case is when the reference spectrum has an absolute minimum. This is the case of the three-dimensional plasmon spectrum. In view of the further discussions, and due to its similarity to the case of ^{4}He, we shall refer to this minimum as the ''roton minimum.'' In this case, we have $\omega_{\mathrm{crit}}(k) = 2\omega_r$, where $\hbar\omega_r$ is the ''roton energy'' located at the wave number k_r. Expanding the energy denominator about this point yields the result

$$\lim_{\hbar\omega\to 2\hbar\omega_r}\Sigma^{\mathrm{CBF}}(k,\omega) = \frac{|V_3(\mathbf{k};-\mathbf{k}-\mathbf{k}_r,\mathbf{k}_r)|^2}{8\pi\rho}\frac{k_r^2\ln(2\hbar\omega_r-\hbar\omega)}{k\varepsilon''(k_r)},\tag{3.45}$$

where $\mathbf{k}_r$ is a vector of length k_r oriented such that the three vectors $\mathbf{k}$, $-\mathbf{k}-\mathbf{k}_r$, and $\mathbf{k}_r$ form an isosceles triangle. In two dimensions, one finds similarly a logarithmic singularity.

To summarize the analysis of this section, we find that we can typically guarantee the existence of collective excitations in the *long-wavelength* regime in both two and three dimensions. An upper bound for these excitations is the Feynman spectrum or the continuum boundary $\hbar\omega_{\mathrm{crit}}(k)$, whichever is lower. We have shown that, when the spectrum has a roton-like structure, one can have collective excitations, even in the long-wavelength limit, *below the plasma frequency*, whereas the plasmon itself can decay for all finite, but infinitesimal wave numbers.

The numerical value of the strength $Z(k)$ of the additional collective mode below the plasmon depends strongly on ''how close'' the solution of the implicit equation (3.37) is to the critical energy $2\hbar\omega_{\mathrm{pl}}$. For long wavelengths, the combination of Eqs. (3.12) and (3.45) yields for the self-energy

$$\Sigma^{\mathrm{CBF}}(k,\omega) = Ck\ln(2\hbar\omega_r-\hbar\omega)$$

$$\text{as } k\to 0+ \quad\text{and}\quad \omega\nearrow 2\omega_r,\tag{3.46}$$

where C is a numerical constant determined by the three-phonon matrix element (3.12) and the kinematic factors appearing in Eq. (3.45). Note that the limits $k\to 0+$ and $\omega\nearrow 2\omega_r$ do not commute, here we must take the limit $\omega\nearrow 2\omega_r$ first for fixed wave number and then evaluate the matrix elements in Eq. (3.45) for small k. As a consequence, we obtain an energy for that ''mode'' of the order $\hbar\omega = 2\hbar\omega_r - \mathrm{const}\times\exp[\hbar(2\omega_R-\omega_p)/Ck]$ and a strength $Z(k)$ that goes to zero as $\exp[\hbar(2\omega_R-\omega_p)/Ck]$ for small k. Clearly this mode is a spurious solution of infinitesimal strength, but the very existence of that solution has, as we shall see, interesting consequences. Exact quantitative statements on the strength of that additional mode for *finite* wave numbers are difficult. We found that the strength of that additional mode is always small compared with the plasmon; the situation is generally very similar to that of ^{4}He, where we have discussed the analytic structure of the self-energy at length.[58,63]

The situation is different for high momentum transfers: the 3D self-energy remains *finite* at the branch cut; cf. Eq. (3.43). This means that the existence of collective excitations can no longer be proven.

F. Plasmon dispersion

In the long-wavelength limit the 3D plasmon dispersion relation is conventionally written as

$$\hbar\omega_0(k) = \hbar\omega_{\mathrm{pl}} + \alpha\frac{\hbar^2k^2}{m} + O(k^4),\tag{3.47}$$

where α is the ''plasmon dispersion coefficient.'' The random phase approximation $\widetilde{V}_{p\text{-}h}(k) = \widetilde{v}(k)$ gives $\alpha = 0$, with a positive fourth-order correction. Chiofalo *et al.*[73] and Moroni *et al.*[38] have used the inequality (3.40) to derive upper bounds for the plasmon dispersion curve. Their results show that the leading dispersion coefficient of the plasmon excitation is negative at all densities due to the negative compressibility of the system.

In our case, we have two sources of the quadratic behavior of the plasmon dispersion relation. One is the momentum dependence of the static particle-hole interaction. For $k\to 0$, the self-energy correction is also proportional to k^2, which leads to a further correction to the plasmon dispersion coefficient. Expanding Eq. (3.37) to first order in k^2, we obtain, using the relationships (3.16) and (3.17),

$$\hbar\omega_0(k) = \hbar\omega_{\mathrm{pl}} + \frac{\hbar^2k^2}{m}\left[\frac{1}{2\rho K_T^{\mathrm{var}}\hbar\omega_{\mathrm{pl}}} + \lim_{k\to 0}\frac{m}{\hbar^2k^2}\Sigma(k,\omega_{\mathrm{pl}})\right]$$

$$= \hbar\omega_{\mathrm{pl}} + \frac{\hbar k^2}{m\omega_{\mathrm{pl}}}\left[\frac{1}{2\rho K_T} + \lim_{k\to 0}\frac{\Sigma(k,\omega_{\mathrm{pl}}) - \frac{1}{2}\Sigma(k,0)}{2S(k)}\right],\tag{3.48}$$

which defines the plasmon dispersion coefficient

$$\alpha = \frac{1}{\hbar\omega_{\mathrm{pl}}}\left[\frac{1}{2\rho K_T} + \lim_{k\to 0}\frac{\Sigma(k,\omega_{\mathrm{pl}}) - \frac{1}{2}\Sigma(k,0)}{2S(k)}\right].\tag{3.49}$$

The above equation has been written in a somewhat suggestive way: the *first* part is directly related to the bulk compressibility, which is negative throughout the whole density range. This part is trivially obtained from the static response function by assuming that the inequality (3.40) is actually an equality. The *second* part is also negative [cf. Eq. (3.39)]; it provides a statement of how much the plasmon dispersion coefficient is lowered through the dynamics of the system.
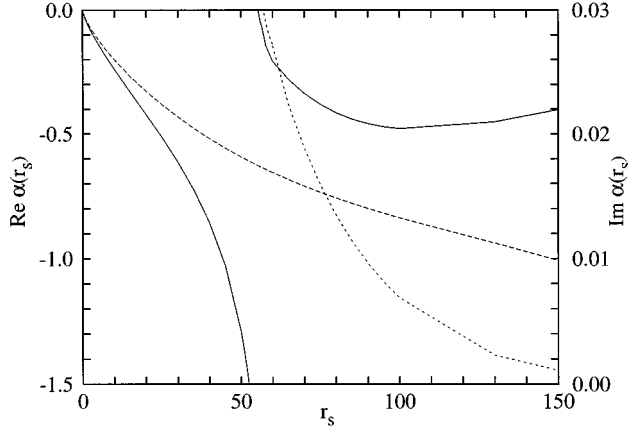
FIG. 14. The real and the imaginary parts of the plasmon dispersion relation are shown, for the three-dimensional charged-boson gas, as a function of r_s. The solid line shows the real part of the full expression (3.49), the long-dashed line the first term, $1/(2\hbar\omega_{pl}\rho K_T)$, and the short-dashed line the imaginary part. Note the different scales applying to the real part (left scale) and the imaginary part (right scale).

We should note, however, that in order to apply the inequality (3.40), one must *assume* that the plasmon is indeed the lowest collective mode. We have shown in the previous section that this is not necessarily true: the long-wavelength limit of the self-energy becomes *complex* if there exists a region of the Feynman spectrum with $2\varepsilon(k) < \hbar\omega_{pl}$. The effect is quite generic and simply states that the plasmon can decay if there is an excitation with a finite momentum, and an energy less than half of the plasmon energy. In other words, the estimate (3.40) becomes invalid for plasmons if

FIG. 15. The normalized dynamic structure function $S(k,\omega)/S(k)$ is shown, for the 3D charged-boson gas, at $r_s = 10$. The strength of $S(k,\omega)/S(k)$ is indicated by the grey scale. Also shown are the Feynman dispersion relations $\varepsilon(k)$ (long-dashed line), the self-energy corrected dispersion relation (solid line), and the continuum boundaries $\hbar\omega_{crit}(k)$ (dotted line). The scale on the right refers to the *relative weight* $Z(k)/S(k)$ (dotted line) and $2m\omega_0(k)Z(k)/(\hbar k^2)$ (dash-dotted line) of the collective mode to the ω^0 and ω^1 sum rules.

$-S(k)/\chi(k,0) < \hbar\omega_{pl}$; from Ref. 38 one would conclude that this happens at $r_s \lesssim 50$, whereas our calculations lead to the slightly larger value $r_s \approx 53$.

Figure 14 shows our calculated plasmon dispersion coefficient and its imaginary part as a function of r_s. Since our reference spectrum is here the Feynman spectrum, the dispersion coefficient becomes complex at a density slightly lower than one would get from the spectra reported in Ref. 38. At that critical r_s value, the real part of the plasmon dispersion coefficient diverges, and the imaginary part becomes nonzero. Below that density, the inequality (3.40) is violated. In that connection, two observations are important: first, our theory satisfies by construction all assumptions that went into the proof.[72] Second, the imaginary part becomes quite small as one moves away from the singularity, and the resonance is indeed almost indistinguishable from a singularity. We also compared our dispersion coefficient with the recent work by Böhm, Conti, and Tosi.[74] We find good agreement with their "best estimate" at $r_s \lesssim 10$ where they find a convergent solution for α.

G. Dispersion relations and dynamic structure function

The collective excitations of the many-particle system are given, in general, by the poles of the response function $\chi(k,\omega)$. The simplest level at which such excited states can be discussed is the Feynman (or random phase) approximation (3.9). In this case, all of the strength of the response function is concentrated in one pole, and the dispersion relation is given by Eq. (2.22). By definition of the Feynman spectrum, there is only one mode of elementary excitations, namely, the plasmon mode. The dispersion curve goes continuously from the plasma frequency $\omega_p = (4\pi\rho e^2/m)^{1/2}$ in the limit $k \to 0$ to the single-particle recoil frequency $\hbar k^2/2m$ at $k \to \infty$.

At a more sophisticated level, self-energy corrections are included in the density-density response function; cf. Eq. (3.7). Two important changes take place: the first is that the dynamic structure function

$$S(k,\omega) = \frac{1}{\pi}\text{Im}\,\chi(k,\omega) \qquad (3.50)$$

is no longer exhausted by a single pole. In general, one writes

$$S(k,\omega) = Z(k)\delta(\omega - \omega_0(k)) + S_{mp}(k,\omega), \qquad (3.51)$$

where $\omega_0(k)$ is the pole of the response function [in our case the solution of Eq. (3.37)], $Z(k)$ the residue of the response function at that point [cf. Eq. (3.38)], and $S_{mp}(k,\omega)$ a "multipair" correction. The second important change is that, under certain circumstances as discussed above, Eq. (3.37) may not have a real solution, in other words, $Z(k)=0$. We discuss therefore the dispersion relation of collective modes, their respective strength, and the multipair excitations simultaneously.

Figure 15 shows the relatively tame situation of $r_s=10$ in three dimensions. In order to make the dynamic structure function more visible at small momentum transfers, the figure shows a grey scale plot of $S(k,\omega)/S(k)$. In this case, the continuum boundary is almost twice the plasma frequency,
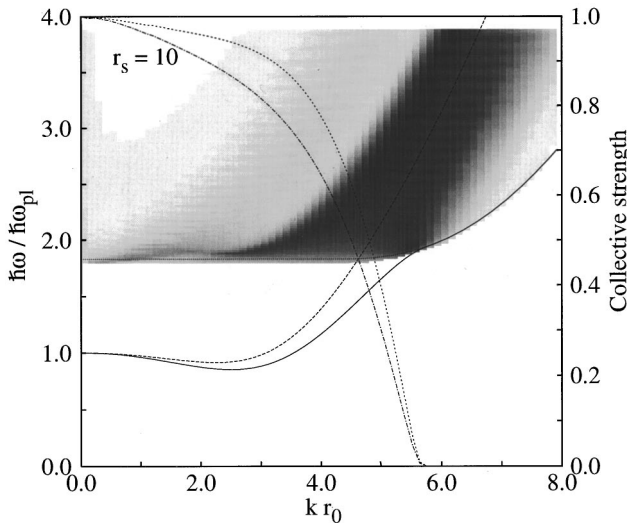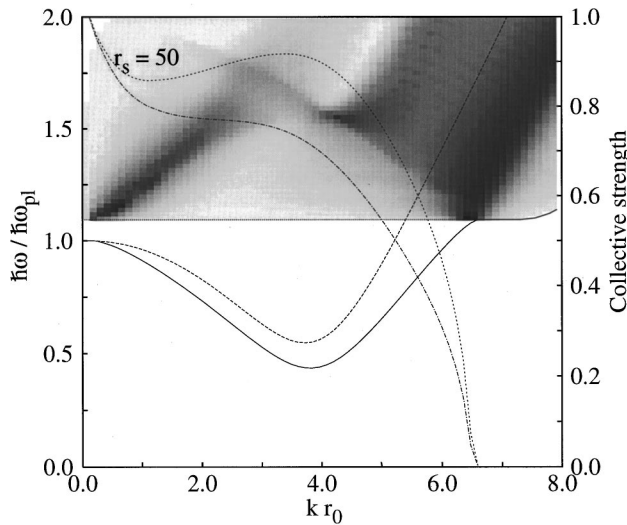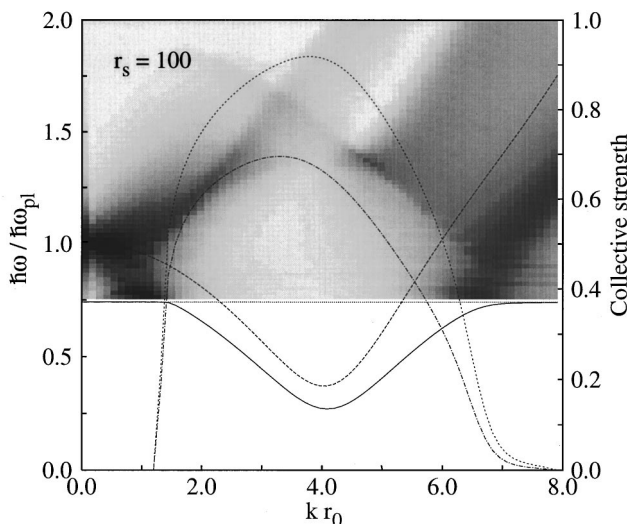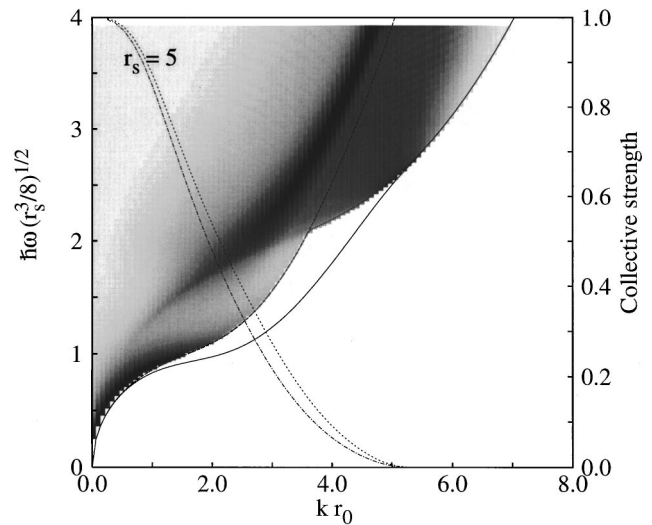
FIG. 16. Same as Fig. 15 for 3D and $r_s = 50$.

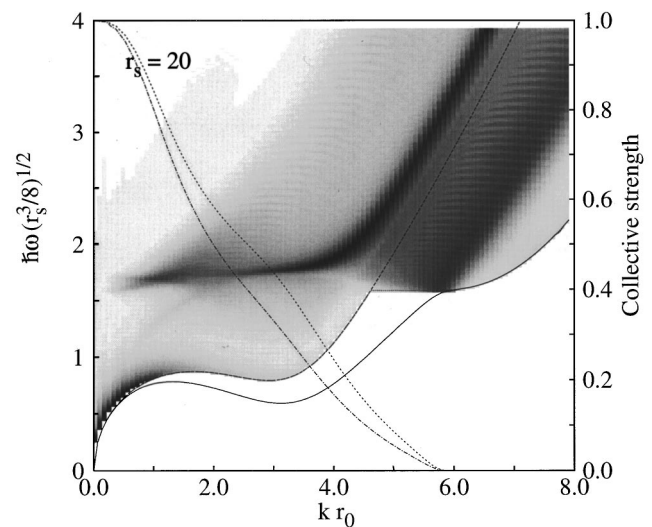FIG. 18. Same as Fig. 15 for 2D and $r_s = 5$.

and up to a momentum transfer of $kr_0 \approx 4$, the Feynman and the CBF spectrum are rather close, and the collective mode exhausts the sum rules (3.36) almost completely. At higher momentum transfers, the Feynman dispersion relation turns into a broad ridge along the single-particle kinetic energy. The rigorously ''collective'' mode loses its strength over a rather small momentum regime, and disappears for $kr_0 > 6$. Note that this corresponds to a regime where no real solutions of Eq. (3.37) exist due to the anomalous dispersion. Figure 15 also gives some justification for the use of the Feynman spectrum in Sec. III B since the actual strength is indeed concentrated around the Feynman spectrum, and not around the solution of Eq. (3.37) or some extrapolation of it to higher momenta.

It was pointed out by Gold[31] that a rotonlike structure—as is familiar from the helium liquids—should also appear in the plasmon dispersion curve of the charged-boson fluid at low densities. The existence of such a minimum follows immediately from the negative plasmon dispersion coefficient; a structure weakly reminiscent of a roton minimum is indeed seen even in the Feynman approximation at $r_s = 10$; see Fig. 15. A much more pronounced roton minimum is seen at

$r_s = 50$; c.f. Fig. 16. In this case, the multipair regime of the dynamic structure function begins slightly above the plasma frequency. At high momentum transfers, $kr_0 > 6.5$, the collective excitation again rapidly loses weight and ultimately disappears. However, we see that the main strength of $S(k, \omega)$ appears to be concentrated along a straight extrapolation of the discrete mode towards higher energies and momenta.

Significant changes happen when the roton minimum drops below half the plasma frequency. Now, the plasmon is, in the long-wavelength limit, *in principle no longer the lowest mode*. A second pole of the response function appears at $2\hbar\omega_r$, where $\hbar\omega_r$ is the roton energy. However, the residue of this pole is, while not exactly zero, practically negligible. The actual strength of $S(k, \omega)$ is located around the plasma frequency, and shifts towards higher momentum transfers and the pole of the CBF response function. At high momentum transfers this collective mode disappears again and continues in a broad ridge around the extrapolation of the collective excitation. To summarize our results in three dimensions, it appears that a well-defined plasmon mode can

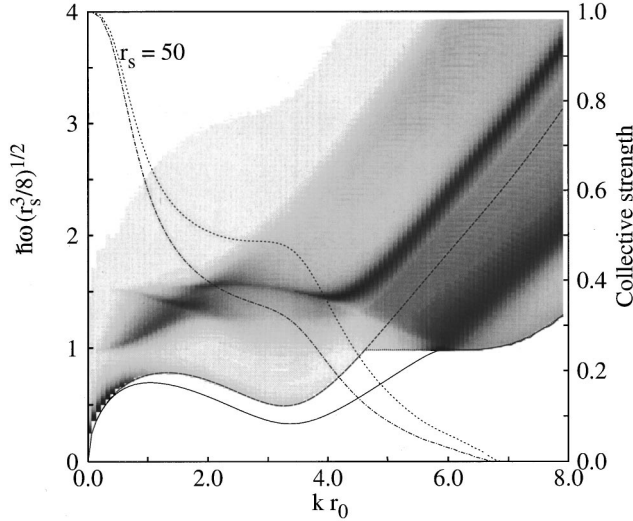FIG. 17. Same as Fig. 15 for 3D and $r_s = 100$.

FIG. 19. Same as Fig. 15 for 2D and $r_s = 20$.

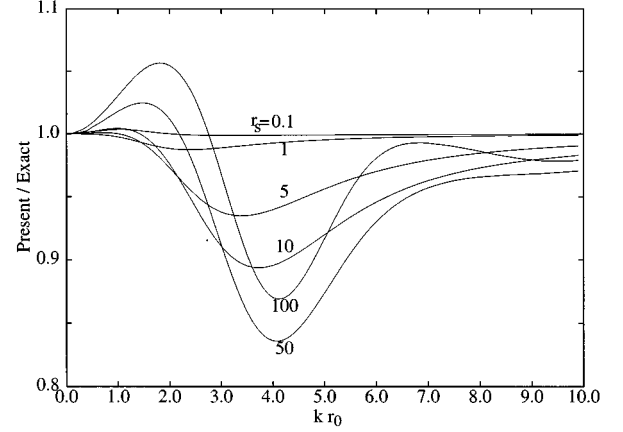FIG. 20. Same as Fig. 15 for 2D and $r_s = 50$.

FIG. 21. The third-moment sum rule from the present calculation divided by the exact result as a function of momentum at different densities labeled with the r_s values.

exist only up to a density for which $\omega_{pl} > 2\omega_r$. In the vicinity of the roton minimum, we always find a well-defined collective mode. Since our analysis of the analytic structure of the self-energy depends to some extent on the comparison between the plasmon and the roton energy as well as on the fact that the roton is well defined, our results should be rather robust against improvements of the theory by, for example, including self-energy corrections in the energy denominator (3.11).

In two dimensions, the plasmon energy approaches zero as $\sqrt{k}$ with the plasma frequency $\omega_p = (2\pi\rho e^2 k/m)^{1/2}$. This result is familiar also from the experimental work done with the 2D electron gas[75] following from the fact that wavelike charge-density perturbations in two dimensions interact like lines of charge while in three dimensions the interaction is between sheets of charge. The $\sqrt{k}$ dispersion relation causes interesting changes from the three-dimensional case. Essentially up to the roton minimum (if it exists), there is no anomalous dispersion and all collective modes are stable. This is reflected in the pole strength $Z(k)$ shown in Figs. 18–20, which extends down to zero in all cases, exhausting the $k^{3/2}$ behavior of the static structure function. Features similar to those in 3D appear at densities low enough (i.e., $r_s > 20$) where a roton minimum develops. This is reflected in a flat continuum boundary at $\omega = 2\omega_r$ above the roton minimum; cf. Figs. 19 and 20. In each of these cases, the actual strength of $S(k,\omega)$ follows a line that appears to be the *extrapolation* of the collective mode into the continuum. We also see another resonance at roughly twice that energy; tentatively we interpret this resonance as a "two-plasmon" excitation, but shall leave its more thorough examination to future studies.

Figures 15–17 and 18–20 also show the relative contribution of the discrete collective mode to the two sum rules (3.36), $Z(k)/S(k)$ and $2m\omega_0(k)Z(k)/(\hbar k^2)$; both ratios are exactly 1 in the Feynman approximation. A number of observations apply: first, the energy-weighted sum rule is exhausted by the collective mode less than the ω^0 sum rule. This is expected since the energy-weighted sum rule places more emphasis on high-energy excitations, which are typically of multiparticle nature. Second, the relative weight of

the collective excitation also decreases at higher momentum transfers. Typically, the collective mode disappears between $kr_0 = 6$ and $kr_0 = 8$ in three dimensions, and between $kr_0 = 5$ and $kr_0 = 6$ in two dimensions and turns into a broad band. At *small* momenta and the low density $r_s \approx 100$ one also sees the consequence of the decay of the long-wavelength plasmons into pairs of rotons: the plasmon itself has a finite width, and a "spurious" collective mode appears at $\omega = 2\omega_r$ that has negligible weight.

H. Third-moment sum rule

We have up to now basically dealt with low-energy excitations. In particular, the theory was *designed* such that the simplest sum rules (3.36) are satisfied identically. The ω^{-1} sum rule may be invoked to calculate the static response function, but since the evaluation of this sum rule needs the dynamic response function for all frequencies, it is easier and more natural to calculate $\chi(k,0)$ from Eq. (3.8). We have also discussed the danger that can come with uncritically adopting sum rule arguments for the estimation of excitation energies; cf. Eq. (3.40) and Fig. 14.

The *third-moment* sum rule is, for the purpose of discussing the nature of the excitation spectrum, of a different nature. The exact form of this sum rule was first derived by Puff.[76] For the charged Bose fluid it can be written in the form[77]

$$\int_{-\infty}^{\infty} S(k,\omega)(\hbar\omega)^3 d(\hbar\omega)$$

$$= 2t(k)[t^2(k) + 4t(k)T/N + 2t(k)\widetilde{v}(k)]$$

$$+ \left(\frac{\hbar^2}{m}\right)^2 \int \frac{d^dq}{(2\pi)^d\rho}(\mathbf{k}\cdot\mathbf{q})^2\widetilde{v}(q)[S(|\mathbf{k}-\mathbf{q}|) - S(q)],$$

(3.52)

where T/N is the exact kinetic energy and $\widetilde{v}(q)$ the Coulomb potential. A form that is suitable for hard-core potentials that have no Fourier transform has been given by Feenberg.[43]

In the present theory, we do *not* expect this sum rule to be exactly satisfied: for it to hold, one must assume that the

spectrum of intermediate states is complete. This is true neither for the one-phonon basis (which leads to the RPA) nor for the two-phonon basis, which leads to the present theory. A second necessary condition for the third-moment sum rule to hold is that the relevant matrix elements are calculated exactly. Again, this is not true in our approximate form of

the self-energy (3.11) and matrix elements (3.12). Thus, the third-moment sum rule can indeed give valuable information on the completeness of the two-phonon basis.

In the evaluation of the third-moment sum rule from the linear response function of Eq. (3.7) we follow the derivation given by Jackson,[62]

$$\int_{-\infty}^{\infty} S(k,\omega)(\hbar\omega)^3 d(\hbar\omega) = 2t(k)\varepsilon^2(k) + 12t(k)\int_0^{\infty}\Gamma(\mathbf{k},\omega)\frac{d\omega}{2\pi} + 4S(k)\int_0^{\infty}\Gamma(\mathbf{k},\omega)[\hbar\omega-\varepsilon(k)]\frac{d\omega}{2\pi}, \tag{3.53}$$

where $\Gamma(\mathbf{k},\omega)$ is the imaginary part of the self-energy,

$$\Gamma(\mathbf{k},\omega) = \frac{\pi}{2}\int\frac{d^dp\,d^dq}{(2\pi)^d\rho}\delta(\mathbf{k}+\mathbf{p}+\mathbf{q})\delta(\hbar\omega-\varepsilon(p)-\varepsilon(q))|V_3(\mathbf{k};\mathbf{p},\mathbf{q})|^2. \tag{3.54}$$

In Fig. 21 we have plotted the ratio of the present and exact results in three dimensions. In the calculation of the exact sum rule we used our structure function and kinetic energy. The comparison shows that the dominant power of Eq. (3.53) in the small-k expansion, $2(\hbar\omega_{\mathrm{pl}})^2k^2$, as well as in the large-k expansion, $(\hbar^2/2m)^3k^6$, is correct. In the high density limit, $r_s \to 0$, the correct expansion is obtained up to the k^4 terms both in the small- and large-wavelength limits,

$$\int_{-\infty}^{\infty}S(\xi,\omega)(\hbar\omega)^3d(\hbar\omega) \approx \begin{cases} 2(12\xi^2+\xi^6)r_s^{-9/2}+0.535386\xi^4r_s^{-15/4}+O(\xi^6)\ \mathrm{Ry}^3 & \text{when } \xi\to0 \\ 2\xi^6r_s^{-9/2}+1.60616\xi^4r_s^{-15/4}+O(\xi^2)\ \mathrm{Ry}^3 & \text{when } \xi\to\infty. \end{cases} \tag{3.55}$$

Here we have used the variable ξ defined in Eq. (2.31). For the correct small-ξ expansion it is essential to include the triplet correlations as was also pointed out in the evaluation of the compressibility.

The deviation from the exact sum rule increases with decreasing density up to $r_s=50$ where a 16% difference was found at $kr_0=4$. As discussed above this is expected due to the approximations in the triplet correlation function and the single-pole form of the self-energy, because the third-moment sum rule heavily weighs the high-energy part of the spectrum. Similar results can be obtained also in two dimensions.

IV. SUMMARY AND OUTLOOK

We have studied in this paper the two- and three-dimensional fluid of charged bosons. We have presented our results for the structure, energetics, and compressibility of the ground state in the light of the triplet correlations included in the trial wave function. Compared with ^{4}He, both the two- and the three-dimensional Bose gas are quite well described by even the simplest version of the HNC/EL theory; in particular the energetics is reproduced within better than 1%. Elementary diagrams and triplet correlations provide an improved consistency of the theoretical description as well as quantitative improvements of derived quantities like the compressibility. As the density is lowered, both the triplet correlations and the elementary diagrams gain importance; this will be of quantitative relevance for our forthcoming studies of Wigner crystallization. We have also carried out extensive comparisons with Monte Carlo results, in particular with the very recent paper by Moroni *et al.* While some quantitative discrepancies remain, we feel that the

overall agreement between HNC/EL results and Monte Carlo data is quite satisfactory.

We have also presented a method for calculating elementary excitations and resonances in these systems. By allowing the interparticle correlations to be time dependent we went beyond the conventional Feynman theory. The theory has been designed in such a manner that those quantities that have been calculated accurately in the ground-state calculation — specifically the $S(k)$ — are not changed any more in the improved theory. In particular, we have assessed the value (or the lack thereof) of sum-rule-based estimates of excitation energies from static properties.

The good agreement of our results with virtually all Monte Carlo data available to us gives us confidence in the validity of our approach to excited states. Concerning the general structure of the dynamic structure function, we believe that the scenario described here is generic, but of course quantitatively improvable in its numerical implementation.[56] It is also possible to study the topological excitations (i.e., vortex structures) using the same basic formalism.[78] These structures have received extensive interest in recent years in connection with the research done with vortices in high-temperature superconductors.

[1] M. R. Schafroth, Phys. Rev. **100**, 463 (1955).

[2] A. S. Alexandrov and N. F. Mott, Supercond. Sci. Technol. **6**, 215 (1993).

[3] N. F. Mott, Comments Condens. Matter. Phys. **16**, 205 (1993).

[4] A. Gold, Physica C **190**, 483 (1992).

[5] A. S. Alexandrov and J. Ranninger, Solid State Commun. **81**, 403 (1992).

[6] A. Kallio, V. Apaja, and S. Pöykkö, Physica B **210**, 472 (1995).

[7] R. Micnas, J. Ranninger, and S. Robaszkiewicz, Rev. Mod. Phys. **62**, 113 (1990).

[8] B. W. Ninham, Phys. Lett. **4**, 278 (1963).

[9] V. L. Ginzburg, J. Stat. Phys. **1**, 3 (1969).

[10] J. P. Hansen, B. Jancovici, and D. Schiff, Phys. Rev. Lett. **29**, 991 (1972).

[11] S. Schramm, K. Langange, and S. E. Koonin, Astrophys. J. **397**, 579 (1992).

[12] H.-M. Müller and K. Langanke, Phys. Rev. C **49**, 524 (1996).

[13] K. S. Singwi, M. P. Tosi, R. H. Land, and A. Sjölander, Phys. Rev. **176**, 589 (1968).

[14] L. J. Lantto and R. Nieminen, Phys. Lett. A **66**, 106 (1978).

[15] J. G. Zabolitzky, Phys. Rev. B **22**, 2353 (1980).

[16] L. I. Foldy, Phys. Rev. **124**, 649 (1961).

[17] K. A. Brueckner, Phys. Rev. **156**, 204 (1967).

[18] D. K. Lee, Phys. Rev. A **2**, 278 (1970).

[19] D. K. Lee and F. H. Ree, Phys. Rev. A **5**, 814 (1972).

[20] R. Monnier, Phys. Rev. A **6**, 393 (1972).

[21] A. A. Caparica and O. Hipólito, Phys. Rev. A **26**, 2832 (1982).

[22] J. Hong and H. J. Choi, Phys. Rev. B **43**, 3238 (1991).

[23] A. S. Alexandrov and W. H. Beere, Physica C **235-240**, 2331 (1994).

[24] A. S. Alexandrov and W. H. Beere, Phys. Rev. B **51**, 5887 (1995).

[25] H.-K. Sim, R. Tao, and F. Y. Wu, Phys. Rev. B **34**, 7123 (1986).

[26] C. I. Um, W. H. Kahng, E. S. Yim, and T. F. George, Phys. Rev. B **41**, 259 (1990).

[27] B. Tanatar and A. K. Das, J. Phys. Condens. Matter **7**, 6065 (1995).

[28] B. Tanatar and A. K. Das, J. Phys. Condens. Matter **8**, 1937 (1996).

[29] S. R. Hore and N. E. Frankel, Phys. Rev. B **12**, 2619 (1975).

[30] D. F. Hines and N. E. Frankel, Phys. Rev. B **20**, 972 (1979).

[31] A. Gold, Z. Phys. B **89**, 1 (1992).

[32] G. Sugiyama, C. Bowen, and B. J. Alder, Phys. Rev. B **46**, 13 042 (1992).

[33] D. M. Kachintsev and S. E. Ulloa, Phys. Rev. B **50**, 8715 (1994).

[34] S. Conti, M. L. Chiofalo, and M. P. Tosi, J. Phys. Condens. Matter **6**, 8795 (1994).

[35] M. Saarela, Phys. Rev. B **29**, 191 (1984).

[36] J.-P. Hansen and R. Mazighi, Phys. Rev. A **18**, 1282 (1978).

[37] D. Ceperley and B. J. Alder, Phys. Rev. Lett. **45**, 566 (1980).

[38] S. Moroni, S. Conti, and M. P. Tosi, Phys. Rev. B **53**, 9688 (1996).

[39] C. E. Campbell, in *Structure of Quantum Fluids* (J. Wiley and Sons, New York, 1978).

[40] W. R. Magro and D. M. Ceperley, Phys. Rev. Lett. **73**, 826 (1994).

[41] E. Krotscheck, Phys. Rev. B **33**, 3158 (1986).

[42] E. Krotscheck and M. Saarela, Phys. Rep. **232**, 1 (1993).

[43] E. Feenberg, *Theory of Quantum Liquids* (Academic, New York, 1969).

[44] C. E. Campbell, Phys. Lett. A **44**, 471 (1973).

[45] C. C. Chang and C. E. Campbell, Phys. Rev. B **15**, 4238 (1977).

[46] A. D. Jackson, A. Lande, and R. A. Smith, Phys. Rep. **86**, 55 (1982).

[47] A. D. Jackson, A. Lande, and R. A. Smith, Phys. Rev. Lett. **54**, 1469 (1985).

[48] E. Krotscheck, R. A. Smith, and A. D. Jackson, Phys. Rev. A **33**, 3535 (1986).

[49] A. Lande and R. A. Smith, Phys. Rev. A **45**, 913 (1992).

[50] A. D. Jackson, A. Lande, R. W. Guitink, and R. A. Smith, Phys. Rev. B **31**, 403 (1985).

[51] D. K. Lee and E. Feenberg, Phys. Rev. **137**, A731 (1965).

[52] F. Rapisarda (private communication).

[53] R. P. Feynman, Phys. Rev. **94**, 262 (1954).

[54] C. C. Chang and C. E. Campbell, Phys. Rev. B **13**, 3779 (1976).

[55] M. Saarela, Phys. Rev. B **33**, 4596 (1986).

[56] M. Saarela and J. Suominen, in *Condensed Matter Theories*, edited by J. S. Arponen, R. F. Bishop, and M. Manninen (Plenum, New York, 1988), Vol. 3, pp. 157–165.

[57] J. Suominen and M. Saarela, in *Condensed Matter Theories*, edited by J. Keller (Plenum, New York, 1989), Vol. 4, p. 377.

[58] B. E. Clements *et al.*, Phys. Rev. B **50**, 6958 (1994).

[59] C. E. Campbell, in *Progress in Liquid Physics*, edited by C. A. Croxton (Wiley, London, 1977), Chap. 6, pp. 213–308.

[60] H. W. Jackson, Phys. Rev. A **4**, 2386 (1971).

[61] H. W. Jackson, Phys. Rev. A **8**, 1529 (1973).

[62] H. W. Jackson, Phys. Rev. A **9**, 964 (1974).

[63] B. E. Clements, E. Krotscheck, and C. J. Tymczak, Phys. Rev. B **53**, 12 253 (1996).

[64] D. Pines and P. Nozieres, *The Theory of Quantum Liquids* (Addison-Wesley, New York, 1990), Vol. II.

[65] C. E. Campbell, R. Folk, and E. Krotscheck, J. Low Temp. Phys. **105**, 13 (1996).

[66] A. Holas, in *Strongly Coupled Plasma Physics*, edited by F. J. Rogers and H. E. DeWitt (Plenum Press, New York, 1986), pp. 463–482.

[67] J. Hubbard, Proc. R. Soc. London Ser. A **276**, 238 (1963).

[68] J. Hubbard, Proc. R. Soc. London Ser. A **277**, 237 (1964).

[69] J. Hubbard, Proc. R. Soc. London Ser. A **281**, 401 (1964).

[70] N. Iwamoto and D. Pines, Phys. Rev. B **29**, 3924 (1984).

[71] N. Iwamoto, E. Krotscheck, and D. Pines, Phys. Rev. B **29**, 3936 (1984).

[72] F. Dalfovo and S. Stringari, Phys. Rev. B **46**, 13 991 (1992).

[73] M. L. Chiofalo, S. Conti, S. Stringari, and M. P. Tosi, J. Phys. Condens. Matter **7**, L85 (1995).

[74] H. M. Böhm, S. Conti, and M. P. Tosi, J. Phys. Condens. Matter **8**, 781 (1996).

[75] C. C. Grimes and G. Adams, Phys. Rev. Lett. **36**, 145 (1976).

[76] R. D. Puff, Phys. Rev. **137**, A406 (1965).

[77] K. N. Pathak and P. Vashishta, Phys. Rev. B **7**, 3649 (1973).

[78] M. Saarela and F. V. Kusmartsev, Phys. Lett. A **202**, 317 (1995).